J. Fluid Mech. (1993), *vol.* 248, *pp.* 1–26

Transonic flow around the leading edge of a thin airfoil with a parabolic nose

By Z. RUSAK

Department of Mechanical Engineering, Aeronautical Engineering and Mechanics, Rensselaer Polytechnic Institute, Troy, NY 12180, USA

(Received 10 May 1991 and in revised form 6 July 1992)

Transonic potential flow around the leading edge of a thin two-dimensional general airfoil with a parabolic nose is analysed. Asymptotic expansions of the velocity potential function are constructed at a fixed transonic similarity parameter (K) in terms of the thickness ratio of the airfoil in an outer region around the airfoil and in an inner region near the nose. These expansions are matched asymptotically. The outer expansion consists of the transonic small-disturbance theory and it second-order problem, where the leading-edge singularity appears. The inner expansion accounts for the flow around the nose, where a stagnation point exists. Analytical expressions are given for the first terms of the inner and outer asymptotic expansions. A boundary value problem is formulated in the inner region for the solution of a uniform sonic flow about an infinite two-dimensional parabola at zero angle of attack, with a symmetric far-field approximation, and with no circulation around it. The numerical solution of the flow in the inner region results in the symmetric pressure distribution on the parabolic nose. Using the outer small-disturbance solution and the nose solution a uniformly valid pressure distribution on the entire airfoil surface can be derived. In the leading terms, the flow around the nose is symmetric and the stagnation point is located at the leading edge for every transonic Mach number of the oncoming flow and shape and small angle of attack of the airfoil. The pressure distribution on the upper and lower surfaces of the airfoil is symmetric near the edge point, and asymmetric deviations increase and become significant only when the distance from the leading edge of the airfoil increases beyond the inner region. Good agreement is found in the leading-edge region between the present solution and numerical solutions of the full potential-flow equations and the Euler equations.

1. Introduction

Transonic potential flow about the leading edge of a round-nosed thin airfoil is a complicated mathematical problem that also causes many difficulties in the numerical calculation of the flow around the entire airfoil (Jameson 1985). An approximation of the velocity potential function of the flow by the transonic small-disturbance theory predicts infinite velocities and pressures near the leading edge of the airfoil. This is known as the transonic 'nose singularity' (Keyfitz, Melnik & Grossman 1978; Cole & Cook 1986). Actually the flow in this region is brought continuously to a stagnation point near the leading edge. Also, comparisons between solutions of the transonic small-disturbance equations and the full potential-flow equations for two-dimensional airfoils (Albone *et al.* 1974; Keyfitz *et al.* 1978) indicated relatively large discrepancies in the nose region of the airfoil. This failure

of the small-disturbance theory is due to the large perturbations to the free stream flow that occur in the leading-edge region. The flow has to be calculated by a more exact theory. A matching between a solution of a compressible stagnation flow around the nose of the airfoil and the transonic small-disturbance theory around the rest of the airfoil may explain the basic character of the flow in the leading-edge region, and be helpful in the numerical calculations of transonic flows about thin airfoils.

The transonic nose singularity that appears in the small-disturbance theory of an airfoil with a parabolic nose was first studied by Nonweiler (1958) and Guderley (1962) and later by Keyfitz *et al.* (1978) and Cole & Cook (1986). The Nonweiler (1958) and Guderley (1962) analyses are limited to the case of a symmetric flow around a slender nose. The first consistent analysis of the problem was given by Keyfitz *et al.* (1978) who described the small-disturbance flow around the leading edge by an asymptotic series of similarity terms. They were determined by a set of boundary value problems and were solved numerically. It was found that the flow is dominated by the thickness effects, where the leading term corresponds to a sonic symmetric flow over a slender parabola at zero incidence. Higher-order terms were described as regular perturbations to the leading term and consisted of either eigenfunction solutions to the problem or of solutions that represent the effects of profile geometry, free-stream speed and local incidence at the nose. It was shown that in the general case, the next possible term after the leading symmetric term corresponds to an eigenfunction that represents an antisymmetric flow around the nose, with an eigenvalue exponent that is very close to the leading-term exponent. Good agreement was found near the nose between the series solution and fully converged numerical solutions of the transonic small-disturbance equation.

On the other hand, Cole & Cook (1986) approximated the dominant term of the perturbation velocity potential near the nose by hodograph similarity solutions of the sonic small-disturbance problem. It was assumed that the hodograph singular solution near the nose is composed of two symmetric and unsymmetric terms of the same leading order, to represent both the thickness and the circulation effects around the nose, as in the case of a subsonic lifting airfoil (Rusak 1990). However, as will be shown later in the present paper, this solution is inconsistent with the tangency boundary condition on the parabolic nose, unless the unsymmetric term is cancelled. It means that the dominant term of the transonic nose singularity is symmetric, and unsymmetric (circulation) effects may be represented only by higher-order terms, as was also found by Keyfitz *et al.* (1978). This result is specifically important when the stagnation flow in an inner region near the parabolic nose of the airfoil is analysed. It results in a dominant symmetric solution in the inner region, where the stagnation point is located at the leading edge.

Kusunose (1979) analysed the inner flow around the nose. Asymptotic expansions of the velocity potential function were constructed in terms of the thickness ratio in an outer region around the leading edge of the airfoil and in an inner region near the nose, and were matched. However, this analysis was based on the inconsistent solution of Cole & Cook (1986). Also, the asymptotic expansions in this analysis are incomplete and the numerical calculations of the flow in the inner region are inconsistent with the results that were found from the matching process.

Despite being an important problem, both theoretically and numerically, the analysis of the transonic potential flow around the leading edge of a thin round-nosed airfoil was never completed. It is expected to be a more complicated problem than the analogous one in the subsonic case, which was recently presented by Rusak

(1990). Both in the outer and inner regions the equations are governed by nonlinear effects, and there are no known solutions to either of these equations. Therefore, asymptotic expansions are used to approximate the solution in the outer region around the leading edge and in the inner region around the parabolic nose.

This paper presents a consistent analysis of the problem. Analytical expressions are given for the first terms of the inner and outer asymptotic expansions and are matched. A uniformly valid pressure distribution on the entire airfoil is obtained. In the leading terms the flow around the nose is symmetric, and to the orders discussed the stagnation point is located at the leading edge for every transonic Mach number of the oncoming flow, for all shapes with a small angle of attack of the airfoil. Asymmetric deviations become significant only when the distance from the leading edge of the airfoil increases beyond the inner region. This special character of the transonic flow about a thin airfoil with a parabolic nose is in direct contrast to the subsonic case, where both symmetric and circulation effects are of the same order in the leading terms, and where the stagnation point shifts along the airfoil's nose due to the circulation around the airfoil (Rusak 1990; Cole 1991). The present solution of the transonic flow around the leading edge of a round-nosed thin airfoil shows good agreement with numerical solutions of the full potential flow equations and the Euler equations.

2. Basic problem and equations

A transonic potential flow about a two-dimensional thin airfoil with a parabolic nose is considered in an (x, y)-plane with unit vectors $(\boldsymbol{e}_x, \boldsymbol{e}_y)$ (figure 1). The airfoil shape is given by

$$B(x,y) = y - \delta F_{\mathrm{u,l}}(x) = 0 \quad \text{for} \quad 0 \leqslant x \leqslant c, \tag{1}$$

where c is the airfoil chord and δ is the thickness ratio, $\delta \ll 1$. The functions $F_{\mathrm{u,l}}(x)$ represent the upper and lower surfaces, respectively. These shape functions are described by

$$F_{\mathrm{u,l}}(x) = C_a(x) - Ax \pm ct(x/c) \quad \text{for} \quad 0 \leqslant x \leqslant c, \tag{2}$$

where $C_a(x)$ is the camber line function, $A = \theta/\delta$, θ is the angle of attack and $ct(x/c)$ is the thickness distribution function. Also, $t(0) = t(1) = 0$ and $C_a(0) = C_a(c) = 0$. Near the leading edge as $x \to 0$ the thickness function changes like $ct(x/c) \sim 2h(cx)^{\frac{1}{2}} + O(x)$ and the camber function changes like $C_a(x) \sim a_1 x + O(x^q)$ with $(q > 1)$, where $R_c = 2h^2\delta^2 c$ is the radius of curvature of the parabolic nose, and a_1 is the local camber of the airfoil at the leading edge (see Abbott & Doenhoff 1959, pp. 111–118).

To the orders considered the flow is irrotational and isentropic. The velocity-potential field Φ of the flow, where $\boldsymbol{q} = \nabla\Phi$ is the velocity vector, is described by the full potential-flow equation:

$$\left.\begin{aligned} &(a^2 - \Phi_x^2)\,\Phi_{xx} - 2\Phi_x \Phi_y \Phi_{xy} + (a^2 - \Phi_y^2)\,\Phi_{yy} = 0, \\ &\frac{a^2}{U^2} = \frac{1}{M_\infty^2} + \frac{\gamma - 1}{2}\left(1 - \frac{\Phi_x^2 + \Phi_y^2}{U^2}\right), \quad M_\infty \equiv \frac{U}{a_\infty}, \end{aligned}\right\} \tag{3}$$

where U, a_∞, M_∞ are the speed of the flow, speed of sound and Mach number of the flow at upstream infinity, respectively, a is the local speed of sound, and γ is the ratio of specific heats. The solution of (3) is sought that satisfies the tangency boundary condition on the airfoil surface,

$$\nabla\Phi \cdot \nabla B = 0 \quad \text{on} \quad B = 0. \tag{4}$$

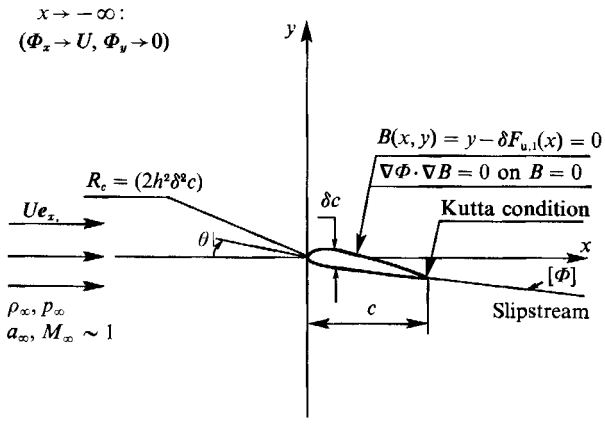

FIGURE 1. Airfoil problem.

Also, disturbances must die out at upstream infinity. As $x \to -\infty$: $(\Phi_x \to U, \Phi_y \to 0)$. The Kutta condition is satisfied at a sharp subsonic trailing edge. In order to get a one-valued potential function the (x,y)-plane is considered as cut along the slipstream that leaves the trailing edge to infinity, where the potential is allowed to jump due to the circulation around the airfoil (figure 1). The density (ρ) and pressure (p) fields of the flow are calculated as function of the velocity $\boldsymbol{q}$ by the isentropic relations and the conditions at upstream infinity ($\rho_\infty, p_\infty, \boldsymbol{q} = U\boldsymbol{e}_x$):

$$\frac{\rho}{\rho_\infty} = \left[1 + \frac{\gamma-1}{2} M_\infty^2 \left(1 - \frac{|\boldsymbol{q}|^2}{U^2}\right)\right]^{1/(\gamma-1)}, \quad \frac{p}{p_\infty} = \left(\frac{\rho}{\rho_\infty}\right)^\gamma. \tag{5}$$

In order to study the transonic flow around the leading edge of a thin airfoil with a parabolic nose, the potential function Φ is approximated by asymptotic expansions in the limit $(\delta \to 0, M_\infty \to 1)$ and with the transonic similarity parameter $K = (1 - M_\infty^2)/(\delta^{\frac{2}{3}} M_\infty^2)$ fixed. An outer expansion is constructed in an outer region around the airfoil. There the coordinates $(x, \tilde{y} = \delta^{\frac{1}{3}} y)$ are fixed as $\delta \to 0$. An inner expansion is constructed in the nose region using stretched coordinates. There $(x^* = x/\delta^2, y^* = y/\delta^2)$ are fixed as $\delta \to 0$.

3. Outer expansion

In the outer region, around the airfoil, the asymptotic expansion of the potential Φ is given in the limit $(\delta \to 0, M_\infty \to 1)$, where

$$1/M_\infty^2 = 1 + K\delta^{\frac{2}{3}} + \ldots$$

and $(x, \tilde{y}; K, A)$ fixed, in the form:

$$\Phi(x, y; M_\infty, A, \delta) = U\{x + \delta^{\frac{2}{3}}\phi_1(x, \tilde{y}; K, A) + \delta^{\frac{4}{3}}\phi_2(x, \tilde{y}; K, A) + O(\epsilon(\delta))\}, \tag{6}$$

where $\epsilon(\delta) \ll \delta^{\frac{4}{3}}$. From the basic system of equations (1)–(5) a sequence of outer problems is found for the solution of the functions ϕ_1 and ϕ_2. The transonic small-disturbance problem for ϕ_1 is given by Cole & Cook (1986):

$$(\gamma+1)\phi_{1x}\phi_{1xx} - \phi_{1\tilde{y}\tilde{y}} = K\phi_{1xx}, \tag{7a}$$

$$\phi_{1\tilde{y}}(x, 0\pm) = F'_{u,l}(x) \quad \text{for} \quad 0 \leqslant x \leqslant c, \tag{7b}$$

$$(\phi_{1x}, \phi_{1\tilde{y}}) \to 0 \quad \text{as} \quad x \to -\infty, \tag{7c}$$

$$\phi_{1x}(c, 0^+) - \phi_{1x}(c, 0^-) = 0 \tag{7d}$$

$$\phi_1(x, 0^+) - \phi_1(x, 0^-) = \Gamma \quad \text{for} \quad x \geqslant c, \tag{7e}$$

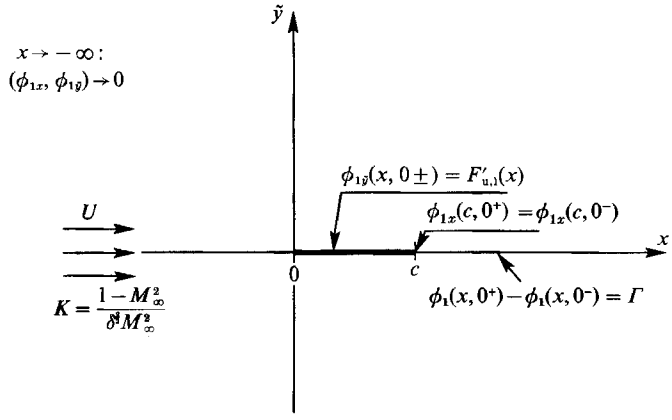

FIGURE 2. Transonic small-disturbance problem.

where Γ is the circulation around the airfoil (figure 2). Shock compression jump conditions should also be satisfied on any shock waves that arise from the solution. The second-order problem for ϕ_2 is

$$(K-(\gamma+1)\phi_{1x})\phi_{2xx}+\phi_{2\tilde{y}\tilde{y}}-(\gamma+1)\phi_{1xx}\phi_{2x}$$
$$=-K\phi_{1\tilde{y}\tilde{y}}+\tfrac{1}{2}(\gamma+1)\phi_{1x}^2\phi_{1xx}+2\phi_{1\tilde{y}}\phi_{1x\tilde{y}}+(\gamma-1)\phi_{1x}\phi_{1\tilde{y}\tilde{y}}, \quad (8a)$$
$$\phi_{2\tilde{y}}(x, 0\pm) = \phi_{1x}(x, 0\pm)F'_{u,1}(x) \quad \text{for} \quad 0\leqslant x\leqslant c, \quad (8b)$$
$$(\phi_{2x}, \phi_{2\tilde{y}})\to 0 \quad \text{as} \quad x\to-\infty. \quad (8c)$$

The pressure coefficient is given by

$$c_p \equiv (p-p_\infty)/(\tfrac{1}{2}\rho_\infty U^2) = -2\delta^{\frac{2}{3}}\phi_{1x}+O(\delta^{\frac{4}{3}}). \quad (9)$$

The solution of (7) in the nose region (as $x\to 0$) is approximated by sum of similarity solutions,

$$(\gamma+1)\phi_1 \sim (\gamma+1)\phi_{1h}+(\gamma+1)\phi_{1p}+\ldots, \quad (10a)$$

where $$(\gamma+1)\phi_{1h} = \tilde{y}^m f(\xi), \quad (\gamma+1)\phi_{1p} = \tilde{y}^a f_p(\xi), \quad \xi = x/\tilde{y}^k, \quad a > m, \quad (10b)$$

and where k, m, a are constants and f, f_p are similarity functions. From (7a) and (10) it is found that in the leading term the flow is near sonic and the effect of the term $(K\phi_{1xx})$ is smaller than the effect of the left-hand side terms in (7a). Therefore, $m = 3k-2$ and $f(\xi)$ is described by the nonlinear differential equation

$$(f_\xi-k^2\xi^2)f_{\xi\xi}-5k(1-k)\xi f_\xi+3(1-k)(3k-2)f = 0. \quad (11)$$

The approximation of the function $f(\xi)$ as a power series as $\tilde{y}\to 0\pm$ and $x > 0$ (as $\xi\to+\infty$) by

$$f(\xi) \sim b_0\xi^{3-2/k}+b_1\xi^{3-3/k}+\ldots \quad (12)$$

results, from the boundary condition for ϕ_1 (equation (7b)), in $k = \frac{6}{7}$ and $b_1 = (\gamma+1)h c^{\frac{1}{2}}$ (Cole & Cook 1986). Therefore,

$$(\gamma+1)\phi_{1h} \sim \tilde{y}^{\frac{4}{7}}f(\xi)+\ldots, \quad \xi = x/\tilde{y}^{\frac{6}{7}}, \quad (13a)$$

where from (11) $$(f_\xi-\tfrac{36}{49}\xi^2)f_{\xi\xi}-\tfrac{30}{49}\xi f_\xi+\tfrac{12}{49}f = 0. \quad (13b)$$

Using (13a) and hodograph similarity solutions, Cole & Cook (1986) found that the singular solution $\tilde{y}$ near the nose can be given by

$$\left.\begin{aligned}\tilde{y} &= c_1\rho^{-\frac{7}{3}}\mathscr{F}(\sin\alpha),\\ \mathscr{F}(\sin\alpha) &\equiv c_2(1-\tfrac{7}{3}\sin^2\alpha)+\sin\alpha F(\tfrac{5}{3}, -\tfrac{1}{2}; \tfrac{3}{2}; \sin^2\alpha),\end{aligned}\right\} \quad (14)$$

where c_1 and c_2 are constants to be determined, F is the standard hypergeometric function (Bateman 1953), and $\mathscr{F}$ is the solution of the hodograph-hypergeometric equation, given in its self-adjoint form by

$$\cos^2\alpha\mathscr{F}''-\tfrac{4}{3}\sin\alpha\mathscr{F}'+\lambda\mathscr{F}=0, \quad \mathscr{F}'\equiv \mathrm{d}\mathscr{F}/\mathrm{d}(\sin\alpha) \tag{15}$$

with $\lambda=\frac{14}{3}$. Also, in (14),

$$\left.\begin{aligned} &\rho^2=v^2-\tfrac{4}{9}\omega^3,\\ &\omega=(\gamma+1)\,\phi_{1hx}=\tilde{y}^{-\frac{2}{7}}f_\xi(\xi),\\ &v=(\gamma+1)\,\phi_{1h\tilde{y}}=\tilde{y}^{-\frac{3}{7}}(\tfrac{4}{7}f(\xi)-\tfrac{6}{7}\xi f_\xi(\xi)),\\ &\sin\alpha=v/\rho. \end{aligned}\right\} \tag{16}$$

The solution $\tilde{y}$ in (14) is given by a linear combination of symmetric and unsymmetric functions, in terms of the hodograph similarity variable, $\sin\alpha$. The parameter α is determined in the range $\alpha_1\leqslant\alpha\leqslant\alpha_3$, where $\alpha_1<0$, α_2 and $\alpha_3>0$ are the first three roots around $\alpha=0$ of the equation $\tilde{y}=0$ or $\mathscr{F}(\sin\alpha)=0$. In the hodograph plane the lines $\alpha=\alpha_1$ and $\alpha=\alpha_3$ represent the boundary curves of the lower and upper surfaces of the airfoil ($\tilde{y}\to 0\pm$, $x>0$) as $x\to 0$. The third (intermediate) solution $\alpha=\alpha_2$ of $\mathscr{F}(\sin\alpha)=0$ ($\alpha_1<\alpha_2<\alpha_3$) represents the x-axis ahead of the airfoil. The three roots $\alpha_1,\alpha_2,\alpha_3$ are functions of the constant c_2 only.

Based on (14) Cole & Cook (1986) believed that to the same leading term the first term of the function $\mathscr{F}$ corresponds to unsymmetric flow around the nose due to circulation, where c_2 is an undetermined circulation parameter as in the case of a subsonic lifting airfoil (Rusak 1990). The second term of the function $\mathscr{F}$ corresponds to the basic symmetric effect of the parabolic nose. This concept was suggested by Cole & Cook (1986) to calculate hodograph-plane solutions of transonic flows around airfoils, where the solution in (14) represented the far-field nose singularity.

From the transformation relations between the transonic physical plane $(x,\tilde{y})$ and the hodograph plane (ρ,α) (Cole & Cook 1986; Müller & Matschat 1964):

$$\partial x/\partial\rho=(\tfrac{3}{2})^{\frac{1}{3}}\rho^{-\frac{2}{3}}\cos^{\frac{1}{3}}\alpha(\partial\tilde{y}/\partial\alpha), \tag{17a}$$

$$Z=1-\tfrac{9}{4}\sigma^2/t^3, \quad W=t^2/\sigma, \tag{17b}$$

where the phase-plane variables (t,σ) are defined by

$$\omega=(x/\tilde{y})^2 t, \quad v=(x/\tilde{y})^3\sigma, \tag{17c}$$

it is found that

$$x=-\tfrac{1}{2}(\tfrac{3}{2})^{\frac{1}{3}}c_1\rho^{-2}\cos^{\frac{4}{3}}\alpha\mathscr{F}', \tag{18a}$$

$$Z=1/\cos^2\alpha, \quad W=3\mathscr{F}/(\sin\alpha\mathscr{F}'). \tag{18b}$$

From (13a), (14) and (18a) the physical similarity variable (ξ) can be given in terms of the hodograph similarity variable ($\sin\alpha$) by

$$\xi=-\tfrac{1}{2}(\tfrac{3}{2})^{\frac{1}{3}}c_1^{\frac{1}{7}}(\cos^{\frac{4}{3}}\alpha\mathscr{F}')/\mathscr{F}^{\frac{6}{7}}. \tag{19}$$

From (17b) and (18b)

$$\left.\begin{aligned} &t=-\tfrac{4}{9}W^2(Z-1)=-(2\mathscr{F}/\cos\alpha\mathscr{F}')^2,\\ &\sigma=(\tfrac{4}{9})^2W^3(Z-1)^2=-\tfrac{8}{3}(2\mathscr{F}/\cos\alpha\mathscr{F}')^3\tan\alpha, \end{aligned}\right\} \tag{20}$$

and from (16), (17), (19) and (20) the similarity function $f(\xi)$ can also be determined in terms of $\sin\alpha$ by

$$f=\tfrac{7}{4}\xi^3(\sigma+\tfrac{6}{7}t)=\tfrac{1}{8}c_1^{\frac{3}{7}}(14\mathscr{F}^{\frac{3}{7}}\sin\alpha+9\mathscr{F}'\cos^2\alpha/\mathscr{F}^{\frac{4}{7}}). \tag{21}$$

Also, it is found that

$$f_\xi = \xi^2 t = -(\tfrac{3}{2})^{\frac{2}{3}} c_1^{\frac{2}{7}} \cos^{\frac{2}{3}}\alpha \mathscr{F}^{\frac{2}{7}} \tag{22a}$$

and from (13*b*), (19), (21) and (22*a*)

$$f_{\xi\xi} = -\tfrac{3}{7}(\tfrac{2}{3})^{\frac{3}{5}} c_1^{\frac{1}{7}} \mathscr{F}^{\frac{1}{7}} \cos^{\frac{1}{3}}\alpha \frac{S-\tan\alpha}{1+S^2}, \quad S \equiv \frac{3\mathscr{F}'\cos\alpha}{7\mathscr{F}}. \tag{22b}$$

Equations (19), (21) and (22) define a parametric representation of the first-order physical similarity solution $f(\xi)$ in terms of the hodograph similarity variable $\sin\alpha$, where α changes in the range $\alpha_1(c_2) \leqslant \alpha \leqslant \alpha_3(c_2)$.

The substitution of (19), (21) and (22) in (16) results in the velocity perturbations in the leading-edge region

$$\left.\begin{aligned} w &= -(\tfrac{3}{2})^{\frac{2}{3}} c_1^{\frac{2}{7}} \tilde{y}^{-\frac{2}{7}} \mathscr{F}^{\frac{2}{7}} \cos^{\frac{2}{3}}\alpha + \ldots, \\ v &= c_1^{\frac{3}{7}} \tilde{y}^{-\frac{3}{7}} \mathscr{F}^{\frac{3}{7}} \sin\alpha + \ldots. \end{aligned}\right\} \tag{23}$$

As $\tilde{y} \to 0\pm$ and $x > 0$ (as $\xi \to \infty$) then $\alpha \to \alpha_{1,3}(c_2)$. From (7*b*), (19) and (23)

$$v(x, 0\pm) = (\tfrac{1}{2})^{\frac{1}{2}} (\tfrac{3}{2})^{\frac{1}{6}} [\sin\alpha \cos^{\frac{2}{3}}\alpha (-\mathscr{F}')^{\frac{1}{2}}]_{\alpha\to\alpha_{1,3}(c_2)} \left(\frac{c_1}{x}\right)^{\frac{1}{2}} + \ldots$$

$$= (\gamma+1) h \left(\frac{c}{x}\right)^{\frac{1}{2}} + \ldots. \tag{24}$$

Therefore,

$$c_1 = 2(\tfrac{2}{3})^{\frac{1}{3}} \frac{(\gamma+1)^2 h^2 c}{[\sin^2\alpha \cos^{\frac{4}{3}}\alpha (-\mathscr{F}')]_{\alpha\to\alpha_{1,3}(c_2)}}. \tag{25}$$

The calculation of $(-\mathscr{F}')_{\alpha\to\alpha_{1,3}(c_2)}$ (Appendix A) shows that

$$c_1 = 2(\tfrac{2}{3})^{\frac{1}{3}} (\tfrac{7}{3} - 1/\sin^2\alpha)_{\alpha\to\alpha_{1,3}(c_2)} (\gamma+1)^2 h^2 c. \tag{26}$$

Since $\alpha_1(c_2) \neq -\alpha_3(c_2)$ for any $c_2 \neq 0$ and the solution has to be continuous across the $(x < 0)$ axis as $\tilde{y} \to 0\pm$, it is found that the tangency boundary condition ((7*b*) or (24)) can be satisfied consistently if and only if:

$$c_2 = 0. \tag{27}$$

This means that the unsymmetric term in the singular solution $\tilde{y}$ in (14) must be cancelled, unlike the concept suggested by Cole & Cook (1986). In (19), (21) and (22);

$$\mathscr{F}(\sin\alpha) = \sin\alpha F(\tfrac{5}{3}, -\tfrac{1}{2}; \tfrac{3}{2}; \sin^2\alpha) \tag{28}$$

and $-\alpha_3 \leqslant \alpha \leqslant \alpha_3$, where α_3 is the first root of the equation $F(\frac{5}{3}, -\frac{1}{2}; \frac{3}{2}; \sin^2\alpha) = 0$, $\alpha_3 = 80.40877922^{2}6°$. Also, $\alpha_2 = 0$ represents the $(-x)$-axis ahead of the nose, and when $\alpha > 0$ then $\tilde{y} > 0$, and vice versa. Equations (13*a*), (21), (23), (28) and (A 2) show that in the leading term the transonic flow field around the parabolic nose is symmetric about the x-axis where:

$$\left.\begin{aligned} (\gamma+1)\phi_1 &= \tilde{y}^{\frac{4}{3}} f(\xi) + \ldots, \\ \xi &= -\tfrac{1}{2}(\tfrac{3}{2})^{\frac{1}{3}} c_1^{\frac{1}{7}} \frac{\cos^{\frac{4}{3}}\alpha F(\frac{5}{3}, -\frac{1}{2}; \frac{1}{2}; \sin^2\alpha)}{\sin^{\frac{6}{7}}\alpha F^{\frac{6}{7}}(\frac{5}{3}, -\frac{1}{2}; \frac{3}{2}; \sin^2\alpha)}, \\ f &= c_1^{\frac{3}{7}} \frac{14\sin^2\alpha F(\frac{5}{3}, -\frac{1}{2}; \frac{3}{2}; \sin^2\alpha) + 9\cos^2\alpha F(\frac{5}{3}, -\frac{1}{2}; \frac{1}{2}; \sin^2\alpha)}{8\sin^{\frac{4}{7}}\alpha F^{\frac{4}{7}}(\frac{5}{3}, -\frac{1}{2}; \frac{3}{2}; \sin^2\alpha)}, \end{aligned}\right\} \tag{29}$$

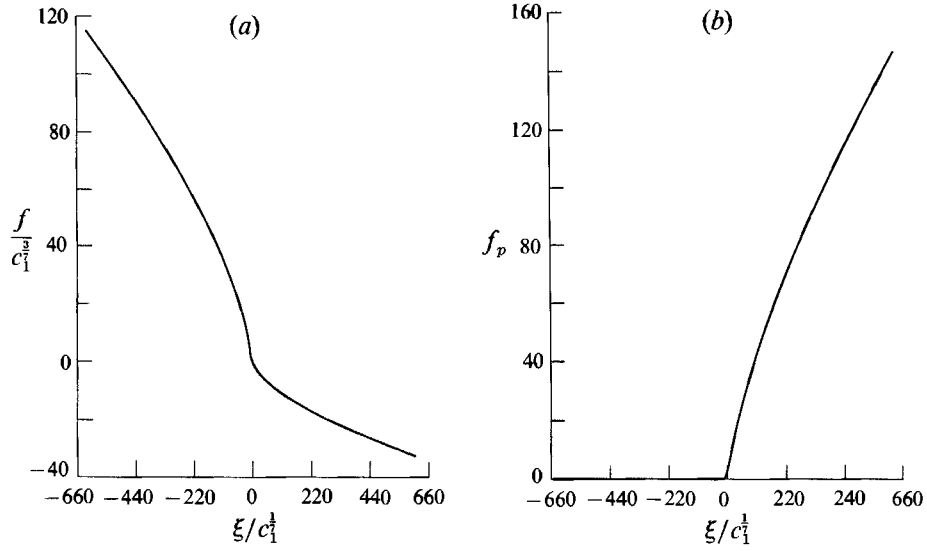

FIGURE 3. (*a*) First-order similarity function $f(\xi)$. (*b*) Second-order similarity function $f_p(\xi)$.

and where, from (25) and (27),

$$c_1 = 2(\tfrac{2}{5})^{\frac{1}{3}}(\tfrac{7}{3} - 1/\sin^2\alpha_3)\,(\gamma+1)^2 h^2 c = 2.2797(\gamma+1)^2 h^2 c. \tag{30}$$

It is clear that $\phi_1(-\tilde{y}, -\alpha) = \phi_1(\tilde{y}, \alpha)$, $\omega(-\tilde{y}, -\alpha) = \omega(\tilde{y}, \alpha)$ and $v(-\tilde{y}, -\alpha) = -v(\tilde{y}, \alpha)$ for any $(\tilde{y}, \alpha)$. The variation of the function $(f/c_1^{\frac{3}{7}})$ with $(\xi/c_1^{\frac{1}{7}})$ is shown in figure 3(*a*). It is a monotonically decreasing function, with a relatively steep gradient about $\xi = 0$. The function $f(\xi)$ can be approximated from (12), (19) and (21) by

$$f(\xi) \sim -(\tfrac{3}{2})^{\frac{5}{3}} \cot^{\frac{2}{3}}\alpha_3 (\gamma+1)^{\frac{2}{3}} h^{\frac{2}{3}} c^{\frac{1}{3}} \xi^{\frac{2}{3}} + (\gamma+1)\, h c^{\frac{1}{2}} \xi^{-\frac{1}{2}} + \ldots \tag{31a}$$

as $\xi \to +\infty$ and by

$$f(\xi) \sim (\tfrac{3}{2})^{\frac{5}{3}} \frac{\cot^{\frac{2}{3}}\alpha_3 (\gamma+1)^{\frac{2}{3}} h^{\frac{2}{3}} c^{\frac{1}{3}} (-\xi)^{\frac{2}{3}}}{\cos^{\frac{10}{9}}\alpha_3 \, F^{\frac{1}{3}}(\frac{5}{3}, -\frac{1}{2}; \frac{1}{2}; \sin^2\alpha_3)} + O((-\xi)^{-\frac{8}{3}}) \tag{31b}$$

as $\xi \to -\infty$. It should be mentioned that the numerical solution of Keyfitz *et al.* (1978) for the function $f(\xi)$ coincides with the analytical parametric representation of this function, given by (29) and (30).

With the dominant term in ϕ_1 being symmetric, it is expected that unsymmetric (circulation) effects may be represented by second-order terms in (10). The substitution of (10) and (13*a*) into (7*a*) results in two possible cases for the solution of the constant a and the function f_p:

$$(f_\xi - \tfrac{36}{49}\xi^2) f_{p\xi\xi} + (f_{\xi\xi} + \tfrac{6}{7}(2a - \tfrac{13}{7})\,\xi) f_{p\xi} - a(a-1) f_p = 0 \tag{32a}$$

when $\frac{4}{7} < a < \frac{6}{7}$, or

$$(f_\xi - \tfrac{36}{49}\xi^2) f_{p\xi\xi} + (f_{\xi\xi} - \tfrac{6}{49}\xi) f_{p\xi} + \tfrac{6}{49} f_p = K f_{\xi\xi} \tag{32b}$$

when $a = \frac{6}{7}$.

Equation (32*a*) is an homogeneous linear equation for f_p while (32*b*) is a forced equation. Since the solution for $f(\xi)$ is determined in (19), (29) and (30) in terms of $\sin\alpha$, (32*a*) is transformed into an equivalent equation for f_p in terms of $\sin\alpha$:

$$\cos^2\alpha f_p'' - \tfrac{4}{3}\sin\alpha f_p' + \tfrac{49}{9} a(a-1) f_p + 2a \frac{\mathscr{F}'\cos^2\alpha}{\mathscr{F}} f_p' + a(a-1)\left(\frac{\mathscr{F}'\cos\alpha}{\mathscr{F}}\right)^2 f_p = 0, \tag{33}$$

where $f'_{\rm p} = {\rm d}f_{\rm p}/{\rm d}(\sin\alpha)$. A detailed derivation of (33) is given in Appendix B. It is interesting to notice that the assumption

$$f_{\rm p} = g(\sin\alpha)\,\mathscr{F}^{-a}(\sin\alpha) \tag{34}$$

results, together with (15), in the linear equation for the function $g(\sin\alpha)$:

$$\cos^2\alpha g'' - \tfrac{4}{3}\sin\alpha g' + \tfrac{49}{9}a(a-\tfrac{1}{7})\,g = 0, \quad g' \equiv {\rm d}g/{\rm d}(\sin\alpha). \tag{35}$$

Equation (35) has the same form as the hodograph-hypergeometric equation for the function $\mathscr{F}(\sin\alpha)$ (equation (15)), but with a different constant λ. Introducing $z \equiv \sin^2\alpha$, (35) takes the form of the standard hodograph-hypergeometric equation (Cole & Cook 1986):

$$z(1-z)\,g_{zz} + (\tfrac{1}{2} - \tfrac{7}{6}z)\,g_z + \frac{\lambda}{4}g = 0, \tag{36a}$$

with

$$\lambda = \tfrac{49}{9}a(a-\tfrac{1}{7}). \tag{36b}$$

Comparing with the standard form of the hypergeometric equation (Bateman 1953), the general family of linearly independent solutions of (36) is given by

$$g = d_1 g_1 + d_2 g_2, \tag{37a}$$

where d_1, d_2 are constants to be determined and

$$g_1 = F\left(\frac{\tilde{a}}{6}, \frac{1-\tilde{a}}{6}; \frac{1}{2}; \sin^2\alpha\right), \quad g_2 = \sin\alpha F\left(\frac{3+\tilde{a}}{6}, \frac{4-\tilde{a}}{6}; \frac{3}{2}; \sin^2\alpha\right), \tag{37b}$$

where again F is an hypergeometric function and $\tilde{a} \equiv 7a$. Therefore, the solution of (32b) is given in terms of $\sin\alpha$ by (34) and (37):

$$f_{\rm p} = [d_1 g_1(\sin\alpha) + d_2 g_2(\sin\alpha)]\,\mathscr{F}^{-\tilde{a}/7}(\sin\alpha), \tag{38}$$

where $\mathscr{F}$ is described by (28). The calculation of the second-order term of the vertical component of the velocity perturbation gives

$$\begin{aligned} v_{\rm p} &\equiv (\gamma+1)\,\phi_{1{\rm p}\tilde{y}} = \tilde{y}^{a-1}(a f_{\rm p} - \tfrac{6}{7}\xi f_{{\rm p}\xi}) \\ &= \tilde{y}^{a-1}\left[a\mathscr{F}^{-a}(d_1 g_1 + d_2 g_2) + \frac{3}{7}\frac{S}{1+S^2}\mathscr{F}^{-(a+1)}(\mathscr{F}(d_1 g'_1 + d_2 g'_2) - a\mathscr{F}'(d_1 g_1 + d_2 g_2))\right], \end{aligned} \tag{39}$$

where S is given by (22b). As $\tilde{y} \to 0\pm$ and $x > 0$ then $\xi \to +\infty$ and $\alpha \to \pm\alpha_3$. From (13a), (19), (22b) and (39) $v_{\rm p}$ is approximated then by

$$v_{\rm p}(x, 0\pm) = -x^{(\tilde{a}-7)/6}\left[(\tfrac{1}{2})^{\frac{7}{6}}(\tfrac{3}{2})^{\frac{7}{18}}c_1^{\frac{1}{6}}\cos^{\frac{14}{9}}\alpha_3\right]^{1-\tilde{a}/7}(-\mathscr{F}')_{\alpha_3}^{\frac{1}{6}-(\tilde{a}/6)}(d_1 g'_1 + d_2 g'_2)_{\alpha\to\pm\alpha_3}. \tag{40}$$

The boundary condition (7b) and the basic assumptions about the airfoil shape result as $\tilde{y} \to 0\pm$ and $x > 0$ in either $v_{\rm p} =$ constant or $v_{\rm p} = 0$. When $v_{\rm p} =$ constant, $a = 1$ results and therefore it is necessary to consider first the case $a = \frac{6}{7}$ (equation (32)). However, when $v_{\rm p} = 0$, (40) gives

$$(d_1 g'_1 + d_2 g'_2)_{\alpha=\pm\alpha_3} = 0, \tag{41a}$$

where from Bateman (1953, p. 102, equations (20) and (22)) it is found that

$$g'_1 = \frac{\tilde{a}(1-\tilde{a})}{9}\sin\alpha F\left(\frac{\tilde{a}}{6}+1, \frac{7-\tilde{a}}{6}; \frac{3}{2}; \sin^2\alpha\right), \quad g'_2 = F\left(\frac{3+\tilde{a}}{6}, \frac{4-\tilde{a}}{6}; \frac{1}{2}; \sin^2\alpha\right). \tag{41b}$$

A numerical calculation of g_1' and g_2' at $|\alpha| = \alpha_3$ shows that $g_1' > 0$ for every $2 \leqslant \tilde{a} \leqslant 7$, whereas g_2' decreases monotonically and changes its sign in this range. It is found that the boundary condition (41*a*) can be satisfied only when $d_1 = 0$ and $g_2' = 0$ at $\alpha = \pm\alpha_3$. Then:

$$\tilde{a} = 4.221\,887\,8104\ldots, \quad a = \tfrac{1}{7}\tilde{a} = 0.603\,127\ldots < \tfrac{6}{7}. \tag{42}$$

This same power of the second-order unsymmetric similarity term was also calculated numerically by Keyfitz *et al.* (1978). The constant d_2 remains undetermined. Equations (10*b*), (22), (37), (38) and (42) show that the next higher-order term of the transonic flow field about the parabolic nose is an unsymmetric circulation function around the leading edge of the airfoil:

$$\begin{aligned}(\gamma+1)\,\phi_{1\mathrm{p}} &= \tilde{y}^{a} f_{\mathrm{p}}(\xi)\\ &= d_2\,\tilde{y}^{\tilde{a}/7}\sin\alpha F\left(\frac{3+\tilde{a}}{6}, \frac{4-\tilde{a}}{6}; \frac{3}{2}; \sin^2\alpha\right)[\sin\alpha F(\tfrac{5}{3}, -\tfrac{1}{2}; \tfrac{3}{2}; \sin^2\alpha)]^{-\tilde{a}/7}\\ &= d_2\,\tilde{y}^{0.6031}(\sin\alpha)^{0.3969} F(1.2036, -0.0370; \tfrac{3}{2}; \sin^2\alpha) F^{-0.6031}(\tfrac{5}{3}, -\tfrac{1}{2}; \tfrac{3}{2}; \sin^2\alpha),\end{aligned} \tag{43}$$

where d_2 is a circulation parameter that can be determined only from the complete solution of the small-disturbance problem described by (7). It is clear that $\phi_{1\mathrm{p}}(-\tilde{y}, -\alpha) = -\phi_{1\mathrm{p}}(\tilde{y}, \alpha)$ for any $(\tilde{y}, \alpha)$. The higher-order terms of the velocity perturbations are

$$\left.\begin{aligned} w_{\mathrm{p}} &= (\gamma+1)\,\phi_{1\mathrm{p}x} = \frac{d_2}{c_1^{\frac{1}{7}}}\frac{3}{7}\left(\frac{2}{3}\right)^{\frac{1}{3}} \tilde{y}^{(\tilde{a}-6)/7}\,\mathscr{F}^{-(\tilde{a}+8)/7}\,\frac{(\mathscr{F}g_2' - (\tilde{a}/7)\mathscr{F}' g_2)}{1+S^2},\\ v_{\mathrm{p}} &= (\gamma+1)\,\phi_{1\mathrm{p}\tilde{y}} = d_2\,\tilde{y}^{(\tilde{a}/7)-1}\mathscr{F}^{-(\tilde{a}/7)-1}\left[\frac{\tilde{a}}{7}\mathscr{F} g_2 + \frac{3}{7}\frac{S}{1+S^2}\left(\mathscr{F} g_2' - \frac{\tilde{a}}{7}\mathscr{F}' g_2\right)\right], \end{aligned}\right\} \tag{44}$$

where S is given by (22*b*). Since both $\mathscr{F}$ and g_2 are antisymmetric functions of α, and therefore $\mathscr{F}'$ and g_2' are symmetric functions of α, it is clear that $w_{\mathrm{p}}(-\tilde{y}, -\alpha) = -w_{\mathrm{p}}(\tilde{y}, \alpha)$ and $v_{\mathrm{p}}(-\tilde{y}, -\alpha) = v_{\mathrm{p}}(\tilde{y}, \alpha)$, as a circulation function should change. The variation of the function (f_{p}) with $(\xi/c_1^{\frac{1}{7}})$ is described in figure 3(*b*). It is a monotonically increasing function; as $\xi \to -\infty$ then $f_{\mathrm{p}} \to 0$ like $(-\xi)^{-\tilde{a}/6}$, for $\xi < 0$ it has relatively small values, and as $\xi \to \infty$ then f_{p} increases like $\xi^{\tilde{a}/6}$.

From (19) and (44), as $\tilde{y} \to 0\pm$ and $x > 0$

$$w_{\mathrm{p}} \sim \pm d_2 C x^{(\tilde{a}/6)-1} = \pm d_2 C x^{-0.2964}, \tag{45}$$

where $$C = \tfrac{7}{3}(\tfrac{2}{3})^{\tilde{a}/18}(\tfrac{1}{2})^{1-\tilde{a}/6} c_1^{-\tilde{a}/42}(\cos\alpha_3)^{-(\frac{3}{7}+\tilde{a}/18)}(-\mathscr{F}')_{\alpha_3}^{-\tilde{a}/6} g_2(\alpha_3) > 0.$$

On the other hand, as $\tilde{y} \to 0\pm$ and $x < 0$ then $\xi \to -\infty$ and $\alpha \to 0$. Then, $w_p = 0$ and

$$v_{\mathrm{p}}(x, 0\pm) \sim d_2 D(-x)^{(\tilde{a}-7)/6} = d_2 D(-x)^{-0.4630}, \tag{46}$$

where $$D = [(\tfrac{1}{2})^{\frac{7}{6}}(\tfrac{3}{2})^{\frac{7}{16}} c_1^{\frac{1}{6}}]^{1-(\tilde{a}/7)} > 0.$$

To summarize, the transonic small-disturbance velocity potential can be approximated in the nose region by

$$(\gamma+1)\,\phi_1 \sim \tilde{y}^{\frac{4}{7}} f(\xi) + \tilde{y}^{4.2219/7} f_{\mathrm{p}}(\xi) + \ldots, \quad \xi = x/\tilde{y}^{\frac{6}{7}}, \tag{47}$$

where the similarity variable ξ and the functions f and f_{p} and are given by (19), (21), (28), (30), (42), (43). It should be emphasized that the first term represents the basic

symmetric flow due to the parabolic nose, and the second term represents the basic unsymmetric flow due to circulation. Although the two terms have different powers, it should be noted that these powers are relatively close. Higher-order terms of the potential ϕ_1 are affected by the combined interaction of the two first basic terms. It can be shown that the next term should be of $O(\tilde{y}^{(2\tilde{a}-4)/7}) = O(\tilde{y}^{4.4438/7})$. It is also clear that the potential ϕ_1 contains in the approximation the term $xK/(\gamma+1) = \tilde{y}^{\frac{6}{7}}\xi K/(\gamma+1)$ which is a special solution of the transonic small-disturbance problem. The pressure distribution along the nose resulting from the approximation to the transonic small-disturbance potential ϕ_1, (47), is given by (9), (31*a*) and (44):

$$c_p \sim 2\delta^{\frac{2}{3}}\left\{\left(\frac{3}{2}\right)^{\frac{2}{3}}\cot^{\frac{2}{3}}\alpha_3(\gamma+1)^{-\frac{1}{3}}h^{\frac{2}{3}}c^{\frac{1}{3}}x^{-\frac{1}{3}} \mp d_2 Cx^{-0.2964} + \ldots - \frac{K}{\gamma+1} + \ldots\right\}. \tag{48}$$

The first term in (48) describes the change in the average of the upper and lower pressures near the leading edge, whereas the second term describes the change in the difference between the upper and lower pressures as the leading edge of the airfoil is approached.

In order to complete the approximation of the solution in the outer region it is necessary to approximate the second-order potential ϕ_2 near the leading edge of the airfoil. The need to do so will be clear later on, when the need for an inner region around the nose of the airfoil will be discussed.

The substitution of (47) in (8*a*) and the approximation of ϕ_2 near the airfoil nose also as a sum of similarity solutions:

$$(\gamma+1)\,\phi_2 \sim \frac{1}{\gamma+1}\tilde{y}^n f_1(\xi) + \ldots, \quad \xi = \frac{x}{\tilde{y}^{\frac{6}{7}}} \tag{49}$$

results in dominant terms that give $n = \frac{2}{7}$ and the equation for $f_1(\xi)$:

$$(f_\xi - \tfrac{36}{49}\xi^2)f_{1\xi\xi} + (f_{\xi\xi} - \tfrac{54}{49}\xi)f_{1\xi} + \tfrac{10}{49}f_1 = -\left[(\tfrac{4}{7}f - \tfrac{6}{7}\xi f_\xi)^2 + \frac{2\gamma-1}{6}f_\xi^3\right]_\xi. \tag{50}$$

Equation (50) is a forced linear equation, where the left-hand side is the same as in (32*a*), but with $a = n = \frac{2}{7}$. Therefore, (50) can be transformed into an equivalent equation for f_1 in terms of $\sin\alpha$ (see Appendix C):

$$f_1 = q(\sin\alpha)\,\mathscr{F}^{-\frac{2}{7}}(\sin\alpha), \tag{51a}$$

where

$$\cos^2\alpha q'' - \tfrac{4}{3}\sin\alpha q' + \tfrac{2}{9}q = 2(\tfrac{2}{3})^{\frac{1}{3}}c_1^{\frac{5}{7}}\cos^{\frac{2}{3}}\alpha\{[1+\tfrac{3}{4}(\gamma-\tfrac{1}{2})][\mathscr{F}'\sin^2\alpha + \tfrac{7}{3}\mathscr{F}\sin\alpha] - \tfrac{3}{4}(\gamma-\tfrac{1}{2})\mathscr{F}'\}. \tag{51b}$$

The homogeneous solution of q is given by (37) with $\tilde{a} = 2$:

$$q_{\mathrm{h}} = \bar{d}_1 F(\tfrac{1}{3}, -\tfrac{1}{6}; \tfrac{1}{2}; \sin^2\alpha) + \bar{d}_2 \sin\alpha F(\tfrac{5}{6}, \tfrac{1}{3}; \tfrac{3}{2}; \sin^2\alpha). \tag{52}$$

The particular solution q_{p} is assumed to be given by

$$q_{\mathrm{p}} = q_1(\sin\alpha)\cos^{\frac{8}{3}}\alpha, \tag{53a}$$

where

$$\begin{aligned}\cos^2\alpha q_1'' - \tfrac{20}{3}\sin\alpha q_1' - \tfrac{22}{9}q_1 + \tfrac{16}{3}q_1\sin^2\alpha/\cos^2\alpha \\ = 2(\tfrac{2}{3})^{\frac{1}{3}}c_1^{\frac{5}{7}}\{\cos^{-2}\alpha[1+\tfrac{3}{4}(\gamma-\tfrac{1}{2})][\mathscr{F}'\sin^2\alpha + \tfrac{7}{3}\mathscr{F}\sin\alpha] - \tfrac{3}{4}(\gamma-\tfrac{1}{2})\mathscr{F}'\}.\end{aligned} \tag{53b}$$

The assumption

$$q_1 = d_3\mathscr{F}'(\sin\alpha) + d_4 q_2(\sin\alpha) \tag{54}$$

together with (15) result in the solution for the constant d_3:

$$d_3 = \tfrac{3}{10}(\tfrac{2}{3})^{\frac{1}{3}} c_1^{\frac{5}{7}}[1+\tfrac{3}{4}(\gamma-\tfrac{1}{2})] \tag{55a}$$

and in an equation for the function q_2:

$$d_4\{\cos^2\alpha q_2'' - \tfrac{20}{3}\sin\alpha q_2' - \tfrac{22}{9}q_2 + \tfrac{16}{3}q_2\sin^2\alpha/\cos^2\alpha\} = E\mathscr{F}'/\cos^2\alpha, \tag{55b}$$

where $E = \frac{1}{5}(\frac{2}{3})^{\frac{1}{3}} c_1^{\frac{5}{7}}(\frac{55}{6}-\gamma)$. The forced solution of (55b) is found by assuming that

$$q_2 = q_3(\sin\alpha)\cos^{-2}\alpha, \tag{56a}$$

where

$$d_4\{\cos^2\alpha q_3'' - \tfrac{8}{3}\sin\alpha q_3' - \tfrac{4}{9}q_3\} = E\mathscr{F}'. \tag{56b}$$

The substitution of $z = \sin^2\alpha$ and of (A 2) result in

$$d_4\{z(1-z)q_{3zz} + (\tfrac{1}{2}-\tfrac{11}{6}z)q_{3z} - \tfrac{1}{9}q_3\} = \tfrac{1}{4}EF(\tfrac{5}{3}, -\tfrac{1}{2}; \tfrac{1}{2}; z). \tag{57}$$

Using the standard power series representation of hypergeometric functions (Bateman 1953):

$$F(\tfrac{5}{3}, -\tfrac{1}{2}; \tfrac{1}{2}; z) = \sum_{l=0}^{\infty} \frac{(\frac{5}{3})_l\,(-\frac{1}{2})_l}{(\frac{1}{2})_l\,l!} z^l, \tag{58}$$

where $(a)_l = a(a+1)\ldots(a+l-1)$ and assuming that

$$q_3 = \sum_{n=1} A_n z^n \tag{59}$$

result in, from (57),

$$\begin{gathered} d_4 = \tfrac{1}{2}E, \quad A_1 = 1, \\ A_{n+1} = A_n \frac{n^2+\frac{5}{6}n+\frac{1}{9}}{(n+1)(n+\frac{1}{2})} + \frac{(\frac{5}{3})_n\,(-\frac{1}{2})_n}{2(\frac{1}{2})_n\,n!(n+1)(n+\frac{1}{2})}. \end{gathered} \tag{60}$$

Equations (51)–(60) result in the solution of the function f_1 in terms of $\sin\alpha$:

$$\begin{aligned} f_1 = \mathscr{F}^{-\frac{2}{7}}\Big\{ & \bar{d}_1 F(\tfrac{1}{3}, -\tfrac{1}{6}; \tfrac{1}{2}; \sin^2\alpha) + \bar{d}_2 \sin\alpha F(\tfrac{5}{6}, \tfrac{1}{3}; \tfrac{3}{2}; \sin^2\alpha) \\ & + \tfrac{1}{10}(\tfrac{2}{3})^{\frac{1}{3}} c_1^{\frac{5}{7}}\Big[3(1+\tfrac{3}{4}(\gamma-\tfrac{1}{2}))\mathscr{F}'\cos^{\frac{8}{3}}\alpha \\ & + (\tfrac{55}{6}-\gamma)\cos^{\frac{3}{3}}\alpha\sin^2\alpha\Big(1+\sum_{n=1}^{\infty} A_{n+1}\sin^{2n}\alpha\Big)\Big]\Big\}, \end{aligned} \tag{61}$$

where $-\alpha_3 \leqslant \alpha \leqslant \alpha_3$. The calculation of the vertical velocity perturbation:

$$v_2 \equiv (\gamma+1)\phi_{2\tilde{y}} = \frac{\tilde{y}^{-\frac{5}{7}}}{\gamma+1}[\tfrac{2}{7}f_1 - \tfrac{6}{7}\xi f_{1\xi}] \tag{62}$$

results, as $\tilde{y}\to 0^{\pm}$ and $x > 0$ (as $\xi\to+\infty$) or as $\alpha\to\pm\alpha_3$, in

$$(\gamma+1)\phi_{2\tilde{y}}(x, 0^{\pm}) = -\frac{1}{\gamma+1} x^{-\frac{5}{6}}(\tfrac{1}{2})^{\frac{5}{6}}(\tfrac{3}{2})^{\frac{5}{18}} c_1^{\frac{5}{12}}\cos^{\frac{10}{9}}\alpha_3(-\mathscr{F}')_{\alpha_3}^{-\frac{1}{6}} q'(\pm\alpha_3), \tag{63}$$

where (19), (49) and (51a) were used. The right-hand side of the boundary condition in (8b) can be approximated as $\tilde{y}\to 0\pm$ and $x\to 0^+$ by (19), (23) and (30):

$$(\gamma+1)\phi_{1x}(x, 0^{\pm})F'_{\mathrm{u},1}(x) \approx \mp\frac{1}{\gamma+1} x^{-\frac{5}{6}}(\tfrac{1}{2})^{\frac{5}{6}}(\tfrac{3}{2})^{\frac{17}{18}} c_1^{\frac{5}{6}}\sin\alpha_3\cos^{\frac{16}{9}}\alpha_3(-\mathscr{F}')_{\alpha_3}^{\frac{5}{6}}. \tag{64}$$

Equations (63) and (64) give

$$q'(\pm\alpha_3) = \mp(\tfrac{3}{2})^{\frac{2}{3}}\sin\alpha_3\cos^{\frac{2}{3}}\alpha_3(-\mathscr{F}')_{\alpha_3}c_1^{\frac{5}{7}}. \tag{65}$$

From (51)–(60) and from Bateman (1953, p. 102, equation (20) and (22)),

$$\begin{aligned} q'(\pm\alpha_3) = {} & \mp\tfrac{2}{9}\bar{d}_1\sin\alpha_3 F(\tfrac{4}{3},\tfrac{5}{6};\tfrac{3}{2};\sin^2\alpha) + \bar{d}_2 F(\tfrac{5}{6},\tfrac{1}{3};\tfrac{1}{2};\sin^2\alpha_3) \\ & \mp\tfrac{1}{5}(\tfrac{2}{3})^{\frac{1}{3}}c_1^{\frac{5}{7}}\sin\alpha_3\cos^{\frac{2}{3}}\alpha_3\Big\{2(1+\tfrac{3}{4}(\gamma-\tfrac{1}{2}))(-\mathscr{F}')_{\alpha_3} \\ & -(\tfrac{55}{6}-\gamma)\Big[1+\sum_{n=1}^{\infty}(n+1)A_{n+1}\sin^{2n}\alpha_3 - \frac{\tan^2\alpha_3}{3}\Big(1+\sum_{n=1}^{\infty}A_{n+1}\sin^{2n}\alpha_3\Big)\Big]\Big\}. \end{aligned} \tag{66}$$

Equations (65) and (66) give

$$\bar{d}_1 = \bar{d}c_1^{\frac{5}{7}}, \quad \bar{d}_2 = 0, \tag{67a}$$

where

$$\begin{aligned} \bar{d} = {} & \tfrac{9}{2}c_1^{\frac{5}{7}}\frac{\cos^{\frac{2}{3}}\alpha_3}{F(\frac{4}{3},\frac{5}{6};\frac{3}{2};\sin^2\alpha_3)}\Big\{(\tfrac{3}{2})^{\frac{2}{3}}(-\mathscr{F}')_{\alpha_3} - \tfrac{1}{5}(\tfrac{2}{3})^{\frac{1}{3}}\Big[2(1+\tfrac{3}{4}(\gamma-\tfrac{1}{2}))(-\mathscr{F}')_{\alpha_3} \\ & -(\tfrac{55}{6}-\gamma)\Big(1+\sum_{n+1}^{\infty}(n+1)A_{n+1}\sin^{2n}\alpha_3 - \frac{\tan^2\alpha_3}{3}\Big(1+\sum_{n=1}^{\infty}A_{n+1}\sin^{2n}\alpha_3\Big)\Big)\Big]\Big\}. \end{aligned} \tag{67b}$$

Therefore, the leading term of ϕ_2 near the leading edge is approximated by

$$\begin{aligned} (\gamma+1)\phi_2 \sim {} & \frac{1}{\gamma+1}\tilde{y}^{\frac{2}{7}}f_1(\xi) = \frac{c_1^{\frac{5}{7}}}{\gamma+1}\tilde{y}^{\frac{2}{7}}\mathscr{F}^{-\frac{2}{7}}\Big\{\bar{d}F(\tfrac{1}{3},-\tfrac{1}{6};\tfrac{3}{2};\sin^2\alpha) \\ & +\tfrac{1}{10}(\tfrac{2}{3})^{\frac{1}{3}}\Big[3(1+\tfrac{3}{4}(\gamma-1))\mathscr{F}'\cos^{\frac{8}{3}}\alpha + (\tfrac{55}{6}-\gamma)\cos^{\frac{2}{3}}\alpha\sin^2\alpha\Big(1+\sum_{n=1}^{\infty}A_{n+1}\sin^{2n}\alpha\Big)\Big]\Big\}, \end{aligned} \tag{68}$$

where $-\alpha_3 \leqslant \alpha \leqslant \alpha_3$. Equation (68) shows that in the leading term the second-order potential ϕ_2 of the transonic flow around the parabolic nose is symmetric about the x-axis: $\phi_2(-\tilde{y},-\alpha) = \phi_2(\tilde{y},\alpha)$. Higher-order terms of the potential ϕ_2 are affected by the approximation of ϕ_1 (equation (47)). It can be shown that the next term of ϕ_2 should be of $O(\tilde{y}^{\tilde{a}-2/7}) = O(\tilde{y}^{2.2219/7})$.

The results can be summarized as follows. From (6), (47) and (68), the potential Φ in the outer region can be approximated in the leading-edge region as $\delta\to 0$ and $M_\infty \to 1$ with $(x,\tilde{y};K,A)$ fixed, by the asymptotic expansion

$$\begin{aligned} \Phi \sim U\Big\{x + {} & \frac{\delta^{\frac{2}{3}}}{\gamma+1}[\tilde{y}^{\frac{4}{7}}f(\xi) + \tilde{y}^{4.2219/7}f_{\mathrm{p}}(\xi) + O(\tilde{y}^{4.4438/7})] \\ & + \frac{\delta^{\frac{4}{3}}}{(\gamma+1)^2}[\tilde{y}^{\frac{2}{7}}f_1(\xi) + O(\tilde{y}^{2.2219/7})] + O(\epsilon(\delta))\Big\}, \end{aligned} \tag{69}$$

where the similarity variable $\xi = x/\tilde{y}^{\frac{6}{7}}$. The functions $f(\xi)$, $f_{\mathrm{p}}(\xi)$ and $f_1(\xi)$ are determined by parametric representations in terms of the hodograph similarity variable $\sin\alpha$ where $|\alpha| \leqslant \alpha_3 = 80.40878°$ (equations (19), (28), (29), (43), (60), (61), (67)). Equation (69) shows that in the leading-edge region as both x and $\tilde{y}\to 0$, the velocities in the x- and $\tilde{y}$-directions become singular, specifically on the airfoil surface (as $\alpha\to\pm\alpha_3$). This is the transonic nose singularity. There is also a misordering in the approximation (69) in the magnitude of the disturbance for every ξ when both x and

y are smaller than $\delta^2 h^2 c$. Therefore, a rescaling in the radial direction only is needed, $x^* = x/\delta^2$, $y^* = x/\delta^2$, in order to account for the local flow around the airfoil nose, where a stagnation point exists.

4. Inner expansion

In the inner region, around the parabolic nose, the asymptotic expansion of the potential Φ is given, in the limit $(\delta \to 0,\ M_\infty \to 1)$ where $1/M_\infty^2 = 1 + K\delta^{\frac{2}{3}} + \ldots$ with $(x^*, y^*; K, A)$ fixed, in the form

$$\Phi(x, y; M_\infty, A, \delta) = U\delta^2 \phi_0(x^*, y^*; M_\infty, A). \tag{70}$$

From the basic system of equations (1)–(5) an inner problem is found for the solution of the function ϕ_0 in the (x^*, y^*)-plane:

$$\phi_0(x^*, y^*; M_\infty, A) = x^* + \bar{\phi}_0(x^*, y^*), \tag{71}$$

where

$$\bar{\phi}_{0y^*y^*} - (\gamma+1)\bar{\phi}_{0x^*}\bar{\phi}_{0x^*x^*} = \tfrac{1}{2}(\gamma+1)\bar{\phi}_{0x^*}^2\bar{\phi}_{0x^*x^*} + 2\bar{\phi}_{0y^*}\bar{\phi}_{0x^*y^*} + (\gamma-1)\bar{\phi}_{0x^*}\bar{\phi}_{0y^*y^*}$$
$$+ \tfrac{1}{2}(\gamma-1)\bar{\phi}_{0x^*}^2\bar{\phi}_{0y^*y^*} + 2\bar{\phi}_{0x^*}\bar{\phi}_{0y^*}\bar{\phi}_{0x^*y^*} + \tfrac{1}{2}(\gamma+1)\bar{\phi}_{0y^*}^2\bar{\phi}_{0y^*y^*} + \tfrac{1}{2}(\gamma-1)\bar{\phi}_{0y^*}^2\bar{\phi}_{0x^*x^*}, \tag{72a}$$

$$\bar{\phi}_{0y^*}[x^*, y^* = \pm 2h(cx^*)^{\frac{1}{2}}] \mp \frac{hc^{\frac{1}{2}}}{x^{*\frac{1}{2}}}[1 + \bar{\phi}_{0x^*}[x^*, y^* = \pm 2h(cx^*)^{\frac{1}{2}}]\} = 0, \tag{72b}$$

$$(\bar{\phi}_{0x^*}, \bar{\phi}_{0y^*}) \to 0 \quad \text{as} \quad x^* \to -\infty. \tag{72c}$$

The problem given in (71) and (72) describes, in the (x^*, y^*)-plane, a sonic $(M_\infty = 1)$ uniform flow $U\boldsymbol{e}_{x^*}$ with density and pressure (ρ_∞, p_∞) around an infinite parabola surface $y^* = \pm 2h(cx^*)^{\frac{1}{2}}$ (figure 4). The compressible flow is governed by the full potential equation for $\bar{\phi}_0(x^*, y^*)$ at $M_\infty = 1$ (written in (72) in a detailed form for the next analysis), and by the tangency boundary condition over the parabola surface. The far-field behaviour of $\bar{\phi}_0$ as $|x^*| \to \infty$ or $|y^*| \to \infty$ has to be specified in order to obtain a well-defined problem. The density (ρ^*) and pressure (p^*) of the flow in the inner region are given by

$$\rho^*/\rho_\infty = [1 + \tfrac{1}{2}(\gamma-1)(1 - \phi_{0x^*}^2 - \phi_{0y^*}^2)]^{1/(\gamma-1)}, \quad p^*/p_\infty = (\rho^*/\rho_\infty)^\gamma.$$

In the far field as $|x^*|$ or $|y^*|$ are increased, the potential function $\bar{\phi}_0$ is assumed to be a weakly nonlinear function that is composed of a basic function $\bar{\phi}_{00}$ and a correction function $\bar{\phi}_{01}$ that is much smaller than $\bar{\phi}_{00}$ as $|x^*|$ or $|y^*|$ are increased:

$$\bar{\phi}_0(x^*, y^*) \sim \bar{\phi}_{00}(x^*, y^*) + \bar{\phi}_{01}(x^*, y^*), \tag{73}$$

where the function $\bar{\phi}_{00}$ is found from

$$\left.\begin{aligned} &\bar{\phi}_{00y^*y^*} - (\gamma+1)\bar{\phi}_{00x^*}\bar{\phi}_{00x^*x^*} = 0, \\ &\bar{\phi}_{00y^*}[x^*, y^* = \pm 2h(cx^*)^{\frac{1}{2}}] = \pm \frac{hc^{\frac{1}{2}}}{x^{*\frac{1}{2}}} \quad \text{as} \quad x^* \to \infty, \\ &(\bar{\phi}_{00x^*}, \bar{\phi}_{00y^*}) \to 0 \quad \text{as} \quad (|x^*| \to \infty \text{ or } |y^*| \to \infty). \end{aligned}\right\} \tag{74}$$

The solution of (74) is given by

$$\bar{\phi}_{00} = y^{*\frac{4}{7}} f^*(\xi^*), \quad \xi^* = x^*/y^{*\frac{6}{7}}, \tag{75a}$$

where

$$(f_{\xi^*}^* - \tfrac{36}{49}\xi^{*2})f_{\xi^*\xi^*}^* - \tfrac{30}{49}\xi^* f_{\xi^*}^* + \tfrac{12}{49} f^* = 0. \tag{75b}$$

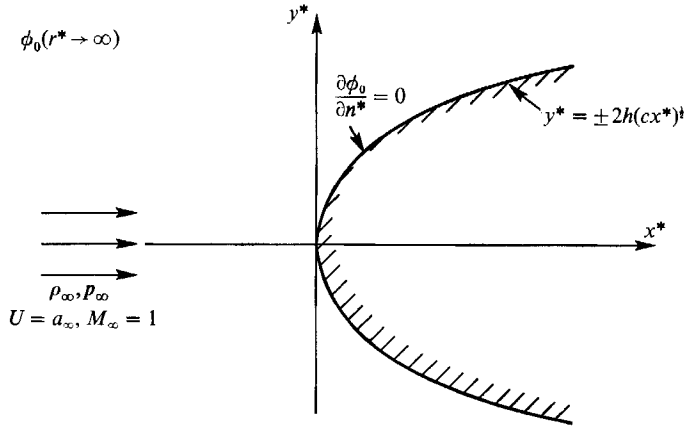

FIGURE 4. Parabolic-nose problem (the inner region).

Equation (75*b*) for $f^*(\xi^*)$ is the same as (13*b*) for $f(\xi)$. Also, the boundary condition in (74) is equivalent to that for ϕ_{1h}. Therefore, $f^*(\xi^*) = f(\xi^*)$, where both ξ^* and f are defined parametrically by $\sin\alpha$, as is $f(\xi)$:

$$\xi^* = -\tfrac{1}{2}(\tfrac{3}{2})^{\frac{1}{3}} c_1^{\frac{1}{3}} \cos^{\frac{4}{3}}\alpha \mathscr{F}'/\mathscr{F}^{\frac{6}{7}}, \tag{76}$$

and f is given by (29) and $|\alpha| \leqslant \alpha_3 = 80.40878°$. The scale parameter c_1 in (76) is taken as the same one that is given by (30), in order to match with the leading term of the outer solution. The function $\bar{\phi}_{01}$ is found by the approximation

$$(\gamma+1)\,\bar{\phi}_{01} \sim \frac{1}{\gamma+1} y^{*l} f_1^*(\xi^*), \quad \xi^* = x^*/y^{*\frac{6}{7}} \tag{77}$$

where $l < \frac{4}{7}$. The function f_1^* is given from (72) and (75) by

$$(f_{\xi^*} - \tfrac{36}{49}\xi^{*2}) f^*_{1\xi^*\xi^*} + [f_{\xi^*\xi^*} + \tfrac{6}{7}(2l - \tfrac{13}{7})\,\xi^*] f^*_{1\xi^*} - a(a-1) f_1^* = 0, \tag{78a}$$

when $\frac{2}{7} < l < \frac{4}{7}$ or by

$$(f_{\xi^*} - \tfrac{36}{49}\xi^{*2}) f^*_{1\xi^*\xi^*} + (f_{\xi^*\xi^*} - \tfrac{54}{49}\xi^*) f^*_{1\xi^*} + \tfrac{10}{49} f_1^* = -\left[(\tfrac{4}{7} f - \tfrac{6}{7}\xi^* f_{\xi^*})^2 + \frac{2\gamma-1}{6} f^3_{\xi^*}\right]_{\xi^*} \tag{78b}$$

when $l = \frac{2}{7}$.

The boundary condition for $\bar{\phi}_{01}$ as $x^* \to \infty$ results, from (72) and (75), in

$$(\gamma+1)\,\bar{\phi}_{01y^*}[x^*, y^* = \pm 2h(cx^*)^{\frac{1}{2}}] = 0 \quad \text{as} \quad x^* \to \infty \tag{79a}$$

or in

$$(\gamma+1)\,\bar{\phi}_{01y^*}[x^*, y^* = \pm 2h(cx^*)^{\frac{1}{2}}]$$

$$= \mp \frac{1}{\gamma+1} x^{*-\frac{5}{6}} (\tfrac{3}{2})^{\frac{17}{18}} c_1^{\frac{5}{6}} \sin\alpha_3 \cos^{\frac{16}{9}}\alpha_3 (-\mathscr{F}')^{\frac{5}{6}}_{\alpha_3} \quad \text{as} \quad x^* \to \infty. \tag{79b}$$

Equation (78*a*) for $f_1^*(\xi^*)$ is equivalent to (32*a*) for $f_p(\xi)$ with l instead of a. Therefore, in the case $\frac{2}{7} < l < \frac{4}{7}$, f_1^* is given by (31) in the form

$$f_1^* = [d_1^* g_1(\sin\alpha) + d_2^* g_2(\sin\alpha)]\,\mathscr{F}^{-\tilde{a}/7}(\sin\alpha), \tag{80}$$

where here $\tilde{a} = 7l$, d_1^* and d_2^* are constants and g_1, g_2 are defined by (37*b*). The calculation of the left-hand side of (79) results as $x^* \to \infty$ in an equivalent expression

to that given on the right-hand side of (40), but with x^* instead of x. The boundary condition in (79a) can be satisfied if and only if

$$(d_1^* g_1' + d_2^* g_2')_{\alpha=\pm\alpha_3} = 0, \tag{81}$$

where g_1', g_2' are given by (41b). However, since both $g_1' \neq 0$ and $g_2' \neq 0$ at $\alpha = \pm\alpha_3$ for every $\tilde{a}$ in the range $2 \leqslant \tilde{a} \leqslant 4$, (81) can be satisfied if and only if $d_1^* = d_2^* = 0$. Therefore, the boundary condition in (79b) can be satisfied if and only if $\tilde{a} = 2$, and then $l = \frac{2}{7}$ and (78b) has to be solved.

Equation (78b) for $f_1^*(\xi^*)$ is the same as (50) for $f_1(\xi)$. Also, the boundary condition in (79b) is equivalent to that for ϕ_2. Therefore, $f_1^*(\xi^*) = f_1(\xi^*)$, where f_1 is given by (68) in terms of $\sin\alpha$. From (70), (71), (75), (76) and (77) the potential Φ in the inner region can be approximated, as $\delta \to 0$ and $M_\infty \to 1$ and as $(|x^*|, |y^*|) \to \infty$, by the asymptotic expansion

$$\Phi \sim U\delta^2 \left\{ x^* + \frac{y^{*\frac{4}{7}}}{\gamma+1} f(\xi^*) + \frac{y^{*\frac{2}{7}}}{(\gamma+1)^2} f_1(\xi^*) + \ldots \right\}, \tag{82}$$

where $\xi^* = x^*/y^{*\frac{6}{7}}$ and f, f_1 are the same functions as in the outer expansion (69).

5. Matching

The matching of the outer and inner asymptotic expansions is carried out with the help of an intermediate region where $x_\eta = x/\eta(\delta)$, $y_\eta = y/\eta(\delta)$ fixed in the limit $\delta \to 0$, $M_\infty \to 1$ as well as the parameters (K, A). The region $\eta(\delta)$ is chosen such that $\delta^2 \ll \eta(\delta) \ll 1$, and as $\delta \to 0$, $\eta(\delta)/\delta^2 \to \infty$. Then $x = \eta(\delta) x_\eta \to 0$ and $\tilde{y} = \delta^{\frac{1}{3}} \eta(\delta) y_\eta \to 0$, whereas $|x^*| = (\eta(\delta)/\delta^2)|x_\eta| \to \infty$ and $|y^*| = (\eta(\delta)/\delta^2)|y_\eta| \to \infty$. Also, $\xi = x/\tilde{y}^{\frac{6}{7}} = (\eta/\delta^2)^{\frac{1}{7}} \xi_\eta$ and $\xi^* = x^*/y^{*\frac{6}{7}} = (\eta/\delta^2)^{\frac{1}{7}} \xi_\eta$, where $\xi_\eta = x_\eta / y_\eta^{\frac{6}{7}}$, so that, in the region $\eta(\delta)$ as $\delta \to 0$, $\xi = \xi^*$. The region $\eta(\delta)$ represents a whole-order class of limits between the inner and outer and is called the overlap region. For matching, the expansions must read the same to a certain order when expressed in the (x_η, y_η) coordinates. From (69) and (82) it is found that:

outer expansion

$$\begin{aligned}\Phi \sim U\Bigg\{ & x + \frac{\delta^{\frac{2}{3}}}{\gamma+1}\Bigg[\delta^{\frac{4}{21}} \eta^{\frac{4}{7}} y_\eta^{\frac{4}{7}} f\left(\left(\frac{\eta}{\delta^2}\right)^{\frac{1}{7}} \xi_\eta\right) \\ & + \delta^{4.2219/21} \eta^{4.2219/7} y^{4.2219/7} f_{\mathrm{p}}\left(\left(\frac{\eta}{\delta^2}\right)^{\frac{1}{7}} \xi_\eta\right) + O(\delta^{4.4438/21} \eta^{4.4438/7} y_\eta^{4.4438/7}) \Bigg)\Bigg] \\ & + \frac{\delta^{\frac{4}{3}}}{(\gamma+1)^2}\left[\delta^{\frac{2}{21}} \eta^{\frac{2}{7}} y_\eta^{\frac{2}{7}} f_1\left(\left(\frac{\eta}{\delta^2}\right)^{\frac{1}{7}} \xi_\eta\right) + O(\delta^{2.2219/21} \eta^{2.2219/7} y_\eta^{2.2219/7}) \right] + O(\epsilon(\delta)) \Bigg\}\end{aligned}$$

$$\Leftrightarrow$$

inner expansion

$$\Phi \sim U\delta^2 \left\{ \frac{x}{\delta^2} + \frac{1}{\gamma+1} \delta^{-\frac{8}{7}} \eta^{\frac{4}{7}} y_\eta^{\frac{4}{7}} f\left(\left(\frac{\eta}{\delta^2}\right)^{\frac{1}{7}} \xi_\eta\right) + \frac{1}{(\gamma+1)^2} \delta^{-\frac{4}{7}} \eta^{\frac{2}{7}} y_\eta^{\frac{2}{7}} f_1\left(\left(\frac{\eta}{\delta^2}\right)^{\frac{1}{7}} \xi_\eta\right) + \ldots \right\}. \tag{83}$$

It is clear that the terms proportional to f and f_1 match. Terms smaller than $O(\delta^{18.2219/21})$ are not matched. By considering these error terms more restrictive bounds on $\eta(\delta)$ are found for a relative error of $(\delta^{\frac{4}{3}})$:

$$\delta^2 \ll \eta(\delta) \ll \delta^{(14-\tilde{a})/3\tilde{a}} = \delta^{0.7720}. \tag{84}$$

The above matching formulates a well-defined boundary-value problem for the solution of the inner compressible flow at $M_\infty = 1$ around the parabolic nose. From (71), (72), (73), (75), (76), (77) the potential $\phi_0(x^*, y^*)$ is found by solving the full potential equation (written in its conservation form for the numerical solution):

$$\nabla^* \cdot \{[1 + \tfrac{1}{2}(\gamma - 1)(1 - \phi_{0x^*}^2 - \phi_{0y^*}^2)]^{1/(\gamma-1)} \nabla^* \phi_0\} = 0, \tag{85a}$$

where $\nabla^* = (\partial/\partial x^*, \partial/\partial y^*)$, and is governed by the satisfaction of the tangency boundary condition over the parabola surface $y^* = \pm 2h\, c^{\frac{1}{2}}(x^* + h^2 c)^{\frac{1}{2}}$:

$$\phi_{0y^*}[x^*, y^* = \pm 2h\, c^{\frac{1}{2}}(x^* + h^2 c)^{\frac{1}{2}}] \mp \frac{h\, c^{\frac{1}{2}}}{(x^* + h^2 c)^{\frac{1}{2}}} \phi_{0x^*}[x^*, y^* = \pm 2h\, c^{\frac{1}{2}}(x^* + h^2 c)^{\frac{1}{2}}] = 0. \tag{85b}$$

The parabola nose was shifted to the point $x^* = -h^2 c$ for the numerical purposes, and by the far-field expansion as $|x^*| \to \infty$ or $|y^*| \to \infty$:

$$\phi_0 \sim x^* + \frac{y^{*\frac{4}{7}}}{\gamma + 1} f(\xi^*) + \frac{y^{*\frac{2}{7}}}{(\gamma + 1)^2} f_1(\xi^*) + \ldots, \quad \xi^* = \frac{x^*}{y^{*\frac{6}{7}}}. \tag{85c}$$

In (85c) ξ^*, f and f_1 are defined parametrically by $\sin\alpha$, where $|\alpha| \leqslant \alpha_3 = 80.40878°$, and are given by (28), (29), (30), (61) and (76). Since the far-field approximation is also symmetric about the x-axis, as is the boundary condition, the solution to (85) for ϕ_0 is symmetric about the x-axis, $\phi_0(x^*, -y^*) = \phi_0(x^*, y^*)$.

6. Numerical solution of the inner flow

The boundary value problem formulated in (85) is solved numerically to calculate the flow around the airfoil parabolic nose, and specifically the pressure distribution on the nose surface. By a transformation to parabolic coordinates:

$$x^* = \tfrac{1}{2}(\bar{\mu}^2 - \bar{\eta}^2), \quad y^* = \bar{\mu}\bar{\eta}, \tag{86}$$

(85) becomes simpler for numerical calculation:

$$\frac{\partial}{\partial \bar{\mu}}(\rho^* \phi_{0\bar{\mu}}) + \frac{\partial}{\partial \bar{\eta}}(\rho^* \phi_{0\bar{\eta}}) = 0 \quad \text{where} \quad \frac{\rho^*}{\rho_\infty} = \left[1 + \frac{\gamma - 1}{2}\left(1 - \frac{\phi_{0\bar{\mu}}^2 + \phi_{0\bar{\eta}}^2}{\bar{\mu}^2 + \bar{\eta}^2}\right)\right]^{1/(\gamma-1)}, \tag{87a}$$

with the tangency boundary condition along the plane $\bar{\eta} = \sqrt{2h\, c^{\frac{1}{2}}}$

$$\phi_{0\bar{\eta}}(\bar{\mu}, \bar{\eta} = \sqrt{2h\, c^{\frac{1}{2}}}) = 0, \tag{87b}$$

and the far-field approximation given by (85c) that can be calculated at any point $(\bar{\mu}, \bar{\eta})$ using (86). The problem can be rescaled by $(h\, c^{\frac{1}{2}})$ so that the plane $\bar{\eta} = \sqrt{2h\, c^{\frac{1}{2}}}$ occurs at $\eta = \sqrt{2}$. Let

$$\eta = \frac{\bar{\eta}}{h\, c^{\frac{1}{2}}}, \quad \mu = \frac{\bar{\mu}}{h\, c^{\frac{1}{2}}}, \quad \phi = \frac{\phi_0}{h^2 c}.$$

Then (87) becomes

$$\frac{\partial}{\partial \mu}(\rho \phi_\mu) + \frac{\partial}{\partial \eta}(\rho \phi_\eta) = 0 \quad \text{where} \quad \rho = \left[1 + \frac{\gamma - 1}{2}\left(1 - \frac{\phi_\mu^2 + \phi_\eta^2}{\mu^2 + \eta^2}\right)\right]^{1/(\gamma-1)}, \tag{88a}$$

$$\phi_\eta(\mu, \eta = \sqrt{2}) = 0. \tag{88b}$$

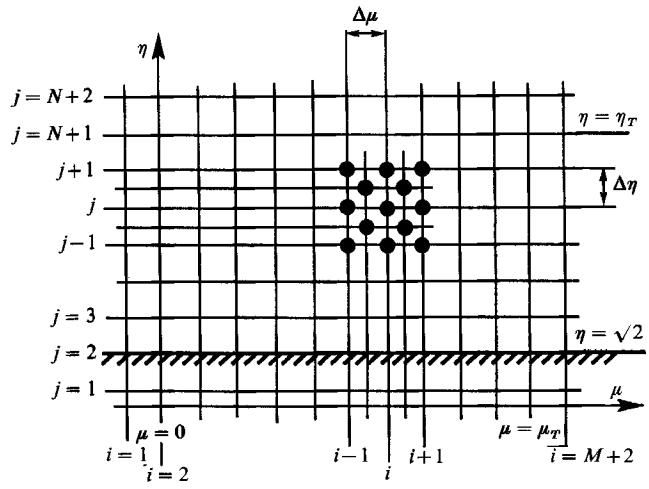

FIGURE 5. Finite difference scheme.

Also, let $X = x^*/h^2c = \frac{1}{2}(\mu^2-\eta^2)$, $Y = y^*/h^2c = \mu\eta$, then $\bar{\xi} \equiv (X+1)/Y^{\frac{6}{7}} = \xi^*/(h^2c)^{\frac{1}{7}}$. From (29), (30) and (76),

$$\bar{\xi} = -\tfrac{1}{2}(\tfrac{3}{2})^{\frac{1}{3}}\left[2(\tfrac{2}{3})^{\frac{1}{3}}\left(\frac{7}{3}-\frac{1}{\sin^2\alpha_3}\right)(\gamma+1)^2\right]^{\frac{1}{7}}\frac{\cos^{\frac{4}{3}}\alpha F(\frac{5}{3},-\frac{1}{2};\frac{1}{2};\sin^2\alpha)}{\sin^{\frac{6}{7}}\alpha F^{\frac{6}{7}}(\frac{5}{3},-\frac{1}{2};\frac{3}{2};\sin^2\alpha)}, \tag{88c}$$

$$\bar{f} \equiv \frac{f}{(h^2c)^{\frac{3}{7}}} = \frac{1}{8}\left[2(\tfrac{2}{3})^{\frac{1}{3}}\left(\frac{7}{3}-\frac{1}{\sin^2\alpha_3}\right)(\gamma+1)^2\right]^{\frac{3}{7}}$$

$$\times\frac{14\sin^2\alpha F(\frac{5}{3},-\frac{1}{2};\frac{3}{2};\sin^2\alpha)+9\cos^2\alpha F(\frac{5}{3},-\frac{1}{2};\frac{1}{2};\sin^2\alpha)}{\sin^{\frac{4}{7}}\alpha F^{\frac{4}{7}}(\frac{5}{3},-\frac{1}{2};\frac{3}{2};\sin^2\alpha)}, \tag{88d}$$

where $|\alpha| \leqslant \alpha_3 = 80.408\,779\,222\,6°$. The far-field approximation is given then by

$$\phi \sim X+\frac{1}{(\gamma+1)}Y^{\frac{4}{7}}\bar{f}(\bar{\xi})+O(Y^{\frac{2}{7}}). \tag{88e}$$

Since ϕ is symmetric about the x-axis the problem can be solved in the half-plane ($\mu \geqslant 0$, $\eta \geqslant \sqrt{2}$) only, by using the symmetry boundary condition along the η-axis:

$$\phi_\mu(0, \eta \geqslant \sqrt{2}) = 0. \tag{88f}$$

A uniform finite difference mesh $(\Delta\mu, \Delta\eta)$ is constructed in the $(\mu \geqslant 0,\ \eta \geqslant \sqrt{2})$-plane (figure 5), with points labelled by (i,j), where $1 \leqslant i \leqslant M+2$ and $1 \leqslant j \leqslant N+2$. The line $j = 2$ is the line $\eta = \sqrt{2}$, the line $j = N+1$ is $\eta = \eta_T$, the line $i = 2$ is $\mu = 0$, and the line $i = M+1$ is $\mu = \mu_T$, where μ_T and η_T are the end values of the computational domain. The lines $i = M+2$ and $j = N+2$ are added to represent the far-field approximation, and the lines $i = 1$ and $j = 1$ for satisfying the boundary conditions along $\eta = \sqrt{2}$ and $\mu = 0$. Equation (88a) can be expressed in a conservative flux form for a box centred on a mesh point at (i,j) as in figure 5. Thus,

$$\frac{(\rho^*\phi_\mu)(i+\frac{1}{2},j)-(\rho^*\phi_\mu)(i-\frac{1}{2},j)}{\Delta\mu}+\frac{(\rho^*\phi_\eta)(i,j+\frac{1}{2})-(\rho^*\phi_\eta)(i,j-\frac{1}{2})}{\Delta\eta} = 0. \tag{89}$$

Since only subsonic speeds are expected in the solution, the various derivatives are approximated by centred finite difference expressions:

$$\left.\begin{aligned}
&\phi_\eta(i,j+\tfrac{1}{2}) = \frac{\phi(i,j+1)-\phi(i,j)}{\Delta\eta}, \quad \phi_\eta(i,j-\tfrac{1}{2}) = \frac{\phi(i,j)-\phi(i,j-1)}{\Delta\eta},\\
&\phi_\mu(i+\tfrac{1}{2},j) = \frac{\phi(i+1,j)-\phi(i,j)}{\Delta\mu}, \quad \phi_\mu(i-\tfrac{1}{2},j) = \frac{\phi(i,j)-\phi(i-1,j)}{\Delta\mu},\\
&\phi_\eta(i\pm\tfrac{1}{2},j) = \frac{1}{2\Delta\eta}(\phi(i\pm1,j+1)+\phi(i,j+1)-\phi(i\pm1,j-1)-\phi(i,j-1)),\\
&\phi_\mu(i,j\pm\tfrac{1}{2}) = \frac{1}{2\Delta\mu}(\phi(i+1,j\pm1)+\phi(i+1,j)-\phi(i-1,j\pm1)-\phi(i-1,j)),
\end{aligned}\right\} \tag{90}$$

and

$$\left.\begin{aligned}
\rho^*(i,j\pm\tfrac{1}{2}) &= \left[1+\frac{\gamma-1}{2}\left(1-\frac{\phi_\eta^2(i,j\pm\tfrac{1}{2})+\phi_\mu^2(i,j\pm\tfrac{1}{2})}{\eta^2(i,j\pm\tfrac{1}{2})+\mu^2(i,j\pm\tfrac{1}{2})}\right)\right]^{1/(\gamma-1)},\\
\rho^*(i\pm\tfrac{1}{2},j) &= \left[1+\frac{\gamma-1}{2}\left(1-\frac{\phi_\eta^2(i\pm\tfrac{1}{2},j)+\phi_\mu^2(i\pm\tfrac{1}{2},j)}{\eta^2(i\pm\tfrac{1}{2},j)+\mu^2(i\pm\tfrac{1}{2},j)}\right)\right]^{1/(\gamma-1)},
\end{aligned}\right\} \tag{91}$$

where

$$\begin{aligned}
&\eta(i,j\pm\tfrac{1}{2}) = \eta(i,j)\pm\tfrac{1}{2}\Delta\eta, \quad \eta(i\pm\tfrac{1}{2},j) = \eta(i,j),\\
&\mu(i,j\pm\tfrac{1}{2}) = \mu(i,j), \quad \mu(i\pm\tfrac{1}{2},j) = \mu(i,j)\pm\tfrac{1}{2}\Delta\mu.
\end{aligned} \tag{92}$$

The substitution of (90) into (89) results in

$$\begin{aligned}
G_{ij} = {}&[\rho^*(i,j+\tfrac{1}{2})(\phi(i,j+1)-\phi(i,j))-\rho^*(i,j-\tfrac{1}{2})(\phi(i,j)-\phi(i,j-1))]\frac{1}{(\Delta\eta)^2}\\
&+[\rho^*(i+\tfrac{1}{2},j)(\phi(i+1,j)-\phi(i,j))-\rho^*(i-\tfrac{1}{2},j)(\phi(i,j)-\phi(i-1,j))]\frac{1}{(\Delta\mu)^2} = 0.
\end{aligned} \tag{93}$$

An iterative point over-relaxation algorithm is used where for an iteration number n:

$$\phi^{(n)}(i,j) = \phi^{(n-1)}(i,j) - \Omega\frac{G_{ij}^{(n-1)}}{(\partial G_{ij}/\partial\phi_{ij})^{(n-1)}} \quad \text{with} \quad 1 \leqslant \Omega < 2, \tag{94}$$

where

$$\begin{aligned}
\frac{\partial G_{ij}}{\partial\phi_{ij}} = {}&-\frac{\rho^*(i,j+\tfrac{1}{2})+\rho^*(i,j-\tfrac{1}{2})}{(\Delta\eta)^2}-\frac{\rho^*(i+\tfrac{1}{2},j)+\rho^*(i-\tfrac{1}{2},j)}{(\Delta\mu)^2}\\
&+\frac{\phi(i,j+1)-\phi(i,j)}{(\Delta\eta)^2}\frac{\partial\rho^*(i,j+\tfrac{1}{2})}{\partial\phi_{ij}}-\frac{\phi(i,j)-\phi(i,j-1)}{(\Delta\eta)^2}\frac{\partial\rho^*(i,j-\tfrac{1}{2})}{\partial\phi_{ij}}\\
&-\frac{\phi(i+1,j)-\phi(i,j)}{(\Delta\mu)^2}\frac{\partial\rho^*(i+\tfrac{1}{2},j)}{\partial\phi_{ij}}-\frac{\phi(i,j)-\phi(i-1,j)}{(\Delta\mu)^2}\frac{\partial\rho^*(i-\tfrac{1}{2},j)}{\partial\phi_{ij}}
\end{aligned} \tag{95a}$$

and

$$\begin{aligned}
\frac{\partial\rho^*(i,j\pm\tfrac{1}{2})}{\partial\phi_{ij}} &= \pm\rho^{*(2-\gamma)}(i,j\pm\tfrac{1}{2})\frac{\phi_\eta(i,j\pm\tfrac{1}{2})}{[\eta^2(i,j\pm\tfrac{1}{2})+\mu^2(i,j\pm\tfrac{1}{2})]}\frac{1}{\Delta\eta}\\
\frac{\partial\rho^*(i\pm\tfrac{1}{2},j)}{\partial\phi_{ij}} &= \pm\rho^{*(2-\gamma)}(i\pm\tfrac{1}{2},j)\frac{\phi_\mu(i\pm\tfrac{1}{2},j)}{[\eta^2(i\pm\tfrac{1}{2},j)+\mu^2(i\pm\tfrac{1}{2},j)]}\frac{1}{\Delta\mu}.
\end{aligned} \tag{95b}$$

The tangency boundary condition (88b) is described with the aid of the line $j = 1$ by

$$\phi(i,1) = \phi(i,3) \quad \text{for every} \quad 2 \leqslant i \leqslant M+1. \tag{96a}$$

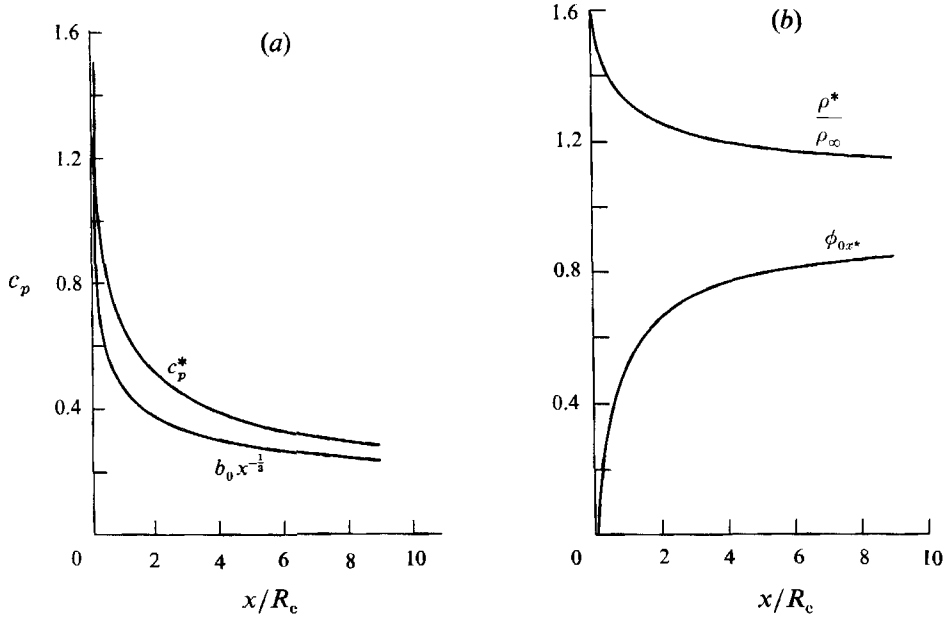

FIGURE 6. (*a*) The pressure distribution along the parabola (c_p^*) and a comparison with the leading term of the pressure distribution from the transonic small-disturbance theory. (*b*) The distribution of the density ratio ρ^*/ρ_∞ and the axial speed ϕ_{0x^*} along the parabola.

The symmetry condition (88*f*) is described with the aid of the line $i = 1$ by

$$\phi(1,j) = \phi(3,j) \quad \text{for every} \quad 2 \leqslant j \leqslant N+1. \tag{96b}$$

The far-field approximation (88*c*, *d*, *e*) is fixed along the lines $i = M+2$ and $j = N+2$. Now, starting with an initial guess for the distribution of the potential ϕ in the computational domain, for example by using the far-field approximation also for the near-field points, the potential ϕ at any point (i,j) in the computational domain ($2 \leqslant i \leqslant M+1$, $2 \leqslant j \leqslant N+1$) can be calculated iteratively using (94). The iterations are repeated until the maximal error is less than a certain small value: $\max|G_{ij}| < \epsilon$. Then the flow field around the parabola is calculated and the pressure distribution (p^*) over the parabolic nose is found by the equation

$$c^*_{p(i,2)} \equiv \frac{p^*-p_\infty}{\frac{1}{2}\rho_\infty U^2} = \frac{2}{\gamma}(\rho^{*\gamma}_{(i,2)}-1) \quad \text{at} \quad \frac{x_i^*}{c} = \tfrac{1}{2}h^2\mu^2_{(i,2)}. \tag{97}$$

The numerical solution of the sonic compressible flow around the parabola is determined by the parameters μ_T, η_T, M, N, Ω and ϵ. The end values of $\mu_T = 40$, $\eta_T = 40+\sqrt{2}$ were used to apply the far-field approximation for ϕ. With these values, the approximation in (88*e*) remains valid, with a small error. The optimal over-relaxation parameter was found to be $\Omega \sim 1.2$ and when the criterion for convergence $\epsilon = 0.003$ was used, the changes in the pressure distribution over the parabola were less than 0.001 with more iterations. The solution tends to converge as the mesh is refined, and when $M = N = 40$ are used the potential function is found within 0.001 of the converged solution (found for the case $M = N = 80$).

The numerical solutions for the pressure distribution over the parabola surface are presented in figure 6(*a*). The pressure coefficient c_p^* is symmetric for the upper and lower parts of the parabola. It starts from a stagnation point value at the leading

edge of the parabola, and decreases monotonically to zero as x is increased. Also shown in figure 7 is the leading term of the pressure distribution resulting from the small-disturbance theory (48). It is evident that near the nose the small-disturbance singular approximation differs from the parabola solution, and only when the distance from the nose is increased do the two solutions tend to match.

7. A uniformly valid solution

A uniformly valid solution for the potential Φ can be constructed from the outer transonic small-disturbance theory for ϕ_1 and ϕ_2 and the parabola inner solution for ϕ_0, by adding the two together and subtracting the common part in the intermediate region where the two solutions match. The composite solution in the limit as $\delta \to 0$ and $M_\infty \to 1$ and with (K, A) fixed is given by

$$\Phi(x, y; M_\infty, A, \delta) \sim U\{x + \delta^{\frac{2}{3}}\phi_1(x, \tilde{y}; K, A) + \delta^{\frac{4}{3}}\phi_2(x, \tilde{y}; K, A) + \delta^2\phi_0(x^*, y^*) - \Phi_{\mathrm{cp}}(x_\eta, y_\eta; \delta, \eta(\delta))\}, \quad (98)$$

where from (83),

$$\Phi_{\mathrm{cp}}(x_\eta, y_\eta; \delta, \eta(\delta)) = \eta x_\eta + \frac{1}{\gamma+1}\delta^{\frac{6}{7}}\eta^{\frac{4}{7}}y_\eta^{\frac{4}{7}}f\left(\left(\frac{\eta}{\delta^2}\right)^{\frac{1}{7}}\xi_\eta\right) + \frac{1}{(\gamma+1)^2}\delta^{\frac{10}{7}}\eta^{\frac{2}{7}}y_\eta^{\frac{2}{7}}f_1\left(\left(\frac{\eta}{\delta^2}\right)^{\frac{1}{7}}\xi_\eta\right). \quad (99)$$

The intermediate region $\eta(\delta)$ must be taken according to (84). The substitution of the composite solution (98) in the isentropic relations (5) results in a uniformly valid pressure distribution over the entire airfoil that is obtained in the limit as $\delta \to 0$ and $M_\infty \to 1$ with (K, A) fixed. The leading terms show that

$$c_p(x; \delta, K, A) = c_p^*(x^*, h) + \frac{\rho^*}{\rho_\infty}\phi_{0x^*}[c_{p_{\mathrm{u,l}}}(x; \delta, K, A) - c_{p\mathrm{cp}}(x; \delta)], \quad (100)$$

where $c_p^*(x^*, h)$, ρ^*/ρ_∞ and ϕ_{0x^*} are calculated from the numerical solution of the parabola problem (inner problem) and are shown in figures 6 (a, b) as functions of the distance along the nose. $c_{p_{\mathrm{u,l}}}(x; \delta, K, A)$ is the outer pressure coefficient on the upper and lower surfaces of the airfoil, (9), and can be approximated by (48) as $x \to 0$ or be calculated by a numerical solution of (7) (Murman & Cole 1971). The common part is given by

$$c_{p\mathrm{cp}}(x; \delta) = 2\delta^{\frac{2}{3}}(\tfrac{3}{2})^{\frac{2}{3}}\cot^{\frac{2}{3}}\alpha_3(\gamma+1)^{-\frac{1}{3}}h^{\frac{2}{3}}c^{\frac{1}{3}}x^{-\frac{1}{3}}. \quad (101)$$

As the leading edge of the airfoil is approached ($x \to 0$ or $0 < x < \delta^2 h^2 c$) the common pressure coefficient ($c_{p\mathrm{cp}}$) cancels the $x^{-\frac{1}{3}}$ singularity of the outer pressure coefficient both on the upper and lower surfaces of the airfoil. Also, in this region ϕ_{0x^*} is small and tends to zero near the stagnation point. Therefore, the dominant term in the leading-edge region is the parabola pressure coefficient c_p^*. The pressure distribution on the upper and lower surfaces of the airfoil is symmetric near the edge point and to the orders discussed the stagnation point is located at the leading edge of the airfoil (at the most forward point of the airfoil against the uniform flow), for every transonic Mach number ($M_\infty \sim 1$) of the oncoming flow and shape and angle of attack of the airfoil. As x is increased beyond the leading-edge region ($x > \delta^{0.772}h^2c$), the density ρ^*/ρ_∞ and the velocity component ϕ_{0x^*} tend to 1 (figure 6 b) and the common pressure coefficient ($c_{p\mathrm{cp}}$) cancels the parabola pressure coefficient (c_p^*). Therefore, the dominant term outside the leading-edge region is the outer pressure coefficient calculated by the transonic small-disturbance theory. In the intermediate region ($\delta^2 h^2 c < x < \delta^{0.772}h^2 c$) the pressure coefficient changes uniformly from c_p^* to $c_{p_{\mathrm{u,l}}}$, and asymmetric deviations from the symmetric inner solution increase and become

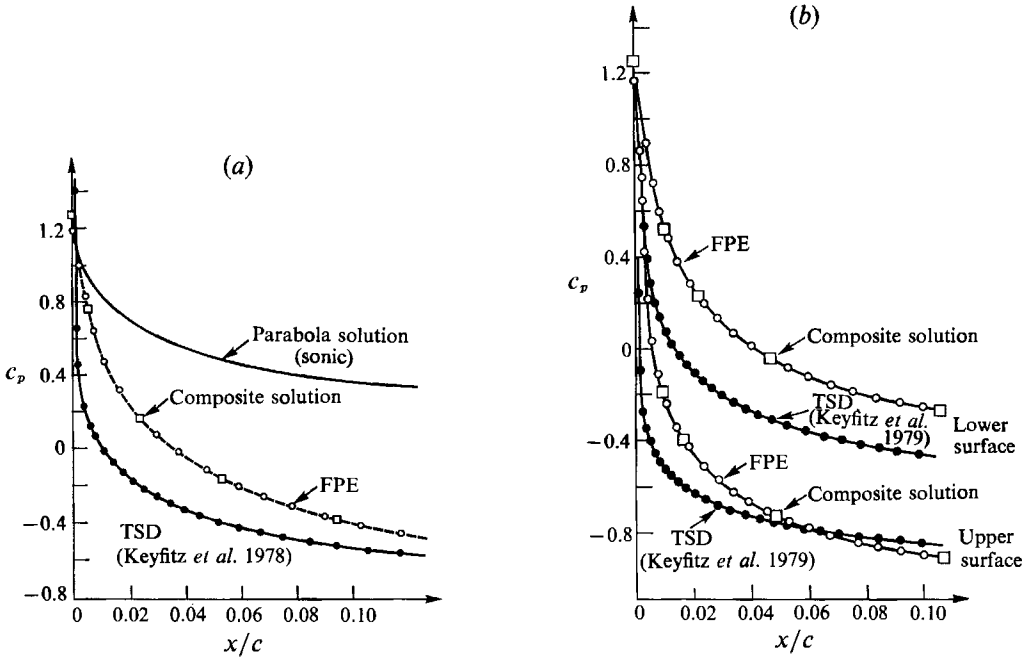

FIGURE 7. The pressure distribution in the leading edge region of a Joukowski airfoil at $M_\infty = 0.8$, $\delta = 0.10$ and (*a*) zero incidence, (*b*) $\theta = 1°$: comparison between several solutions. (FPE: full potential-flow equation; TSD: transonic small-disturbance equations.)

significant as the distance (x) from the leading edge of the airfoil increases beyond the inner region.

The uniformly valid approximation of (100) was applied to calculate the pressure distributions around the leading edge of several airfoils given at various transonic Mach numbers and various angles of attack. Two examples of a transonic flow ($M_\infty = 0.8$) over a symmetric Joukowski airfoil with a thickness ratio of $\delta = 0.1$ at angles of attack $\theta = 0°$ and $1°$ are shown in figures 7(*a*) and 7(*b*). Using the numerical small-disturbance solution of Keyfitz *et al.* (1978) or their analytical approximation for this solution, and the present solution of the parabola sonic problem described in figures 6(*a*) and 6(*b*), the pressure distributions along the nose of the airfoil were calculated. Good agreement is found between the present approximations for the pressure distribution and the numerical solutions of the full potential-flow equations of Keyfitz *et al.* (1978, 1979) (using Bauer *et al's.* 1975 code) over the first 10% of the chord. It is evident that the solution of the transonic small-disturbance equation differs considerably from the full potential-flow solution (this was also indicated by Keyfitz *et al.* 1978), as does the solution of the parabola sonic problem. Only when the composite solution is used, which matches between these two solutions, is a good correlation found with the numerical solution of the full potential-flow equation.

It should be pointed out that in order to get a good approximation to the pressure distribution around the airfoil's nose by using the present theory, it is necessary to use fully converged solutions of the transonic small-disturbance problem. As was already described by Keyfitz *et al.* (1978, 1979), incompletely converged solutions can sometimes display an agreement with the full potential-flow solutions, but it disappears when the mesh is refined. Such incompletely converged solutions may lead to incorrect approximations of the flow around the nose when the present theory is used.

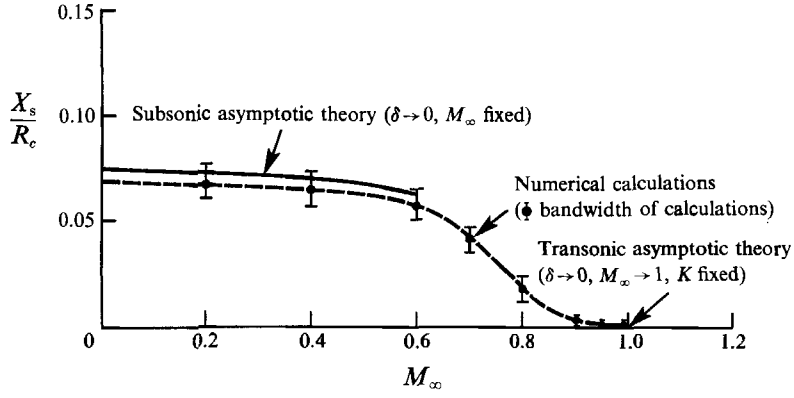

FIGURE 8. The shift of the stagnation point X_s as function of the Mach number M_∞ for a NACA0012 airfoil at angle of attack $\theta = 2°$.

Figure 8 shows the calculated shift of the stagnation point (X_s) along the nose of a NACA0012 airfoil as the Mach number M_∞ is increased from zero to one at a fixed angle of attack $\theta = 2°$. The numerical solutions of the Euler equations were obtained using an adaptive procedure (Webster *et al.* 1992) built on a space–time finite element procedure of Hughes, Franca & Hulbert (1989). The small error tolerance requirement placed on the adaptive procedure forced highly refined meshes around the airfoil's nose, producing highly accurate converged results in that region. It is evident that within the bandwidth of the calculations, there is a good agreement between the subsonic asymptotic solution of Rusak (1990) and the numerical results for $0 < M_\infty < 0.6$. As M_∞ is increased the stagnation point shifts toward the leading edge and is located very close to the most forward point of the airfoil when M_∞ is around 1, as is predicted by the present analysis. The very small gap that is found between the theoretical and the numerical results can be explained by the basic differences between the two solutions. The asymptotic solution was developed in the limit $\delta \to 0$ and $M_\infty \to 1$ with K and A fixed whereas the numerical calculations were carried out with δ fixed ($\delta = 0.12$) when $M_\infty \to 1$. In order to keep K and A fixed in the numerical calculations, as is done in the asymptotic solution, the thickness ratio δ and the angle of attack θ of the airfoil have to be reduced as M_∞ approaches 1.

In the intermediate region around the critical Mach number the numerical results on the change of X_s with M_∞ match between the subsonic and transonic asymptotic solutions (figure 8). This change of X_s with M_∞ has not yet been analysed theoretically. It is expected to describe a uniform change as M_∞ is increased from the subsonic to the transonic regime. The analysis of this problem seems to be more complicated than the present analysis, since it has to match correctly between the subsonic case that is dominated by the total circulation around the airfoil and the transonic case that is governed by the local shape of the parabolic nose.

8. Conclusions

The transonic potential flow about the leading edge of a thin airfoil with a parabolic nose can be analysed by matched asymptotic methods. Asymptotic expansions of the velocity potential function are constructed at a fixed transonic similarity parameter in terms of the airfoil thickness ratio at an outer region around the airfoil and in an inner region near the nose. Analytical expressions are given for the first terms of the inner and outer asymptotic expansions. A previous solution of Cole & Cook (1986) to

the leading-edge singularity resulting from the transonic small-disturbance theory is found inconsistent and is corrected. The matching of the inner and outer expansions results in a well-defined boundary-value problem in the inner region for the solution of a compressible sonic flow around an infinite parabola at zero angle of attack and with a symmetric far-field approximation. The numerical solution of the inner flow results in the symmetric pressure and velocity distributions on the parabolic nose. From the outer and inner solutions a uniformly valid pressure distribution on the entire airfoil surface is derived. In the leading terms, the flow around the nose is symmetric and to the orders discussed the stagnation point is located at the leading edge for every transonic Mach number of the oncoming flow and shape and small angle of attack of the airfoil. The pressure distribution on the upper and lower surfaces of the airfoil is symmetric near the edge point, and asymmetric deviations increase and become significant only when the distance from the leading edge of the airfoil increases beyond the inner region. Numerical solutions of the full potential-flow equations and the Euler equations for round-nosed airfoils are in a good agreement with the results of the present theory.

It is my great pleasure to express my gratitude to Professor Julian D. Cole who suggested this problem to me and provided me with very helpful advice. I would like to thank Mr Bruce E. Webster for his help with the numerical calculations, and Professor T. J. R. Hughes for access to the ENSA space–time finite element code for solving Euler/Navier–Stokes problems developed by his group at Stanford University. This research was carried out with the support of the Air Force Office of Scientific Research under Grant AFOSR 88-0037.

Appendix A

The function $\mathscr{F}(\sin\alpha)$ is given by (14). By introducing $z = \sin\alpha$:

$$\mathscr{F}(z) = c_2(1-\tfrac{7}{3}z^2) + zF(\tfrac{5}{3}, -\tfrac{1}{2}; \tfrac{3}{2}; z^2). \tag{A 1}$$

Using Bateman (1953, p. 102, equation (22))

$$\mathscr{F}' = \mathrm{d}\mathscr{F}/\mathrm{d}z = -\tfrac{14}{3}c_2 z + F(\tfrac{5}{3}, -\tfrac{1}{2}; \tfrac{1}{2}; z^2). \tag{A 2}$$

On the other hand, from Bateman (1953, p. 103, equation (30)),

$$\tfrac{1}{4}(1-z^2)F(\tfrac{5}{3}, -\tfrac{1}{2}; -\tfrac{1}{2}; z^2) + \tfrac{1}{4}(\tfrac{7}{3}z^2-1)F(\tfrac{5}{3}, -\tfrac{1}{2}; \tfrac{1}{2}; z^2) = \tfrac{7}{6}z^2F(\tfrac{5}{3}, -\tfrac{1}{2}; \tfrac{3}{2}; z^2). \tag{A 3}$$

Since $F(\frac{5}{3}, -\frac{1}{2}; -\frac{1}{2}; z^2) = (1-z^2)^{-\frac{2}{3}}$ (Bateman 1953, p. 101, equation (4)), (A 1), (A 2), (A 3) result in

$$\mathscr{F}(z) = \frac{3}{14}\frac{1}{z}[(\tfrac{7}{3}z^2-1)\mathscr{F}' + (1-z^2)^{-\frac{2}{3}}]. \tag{A 4}$$

Therefore, when $\mathscr{F} = 0$ at $\alpha = \alpha_{1,3}(c_2)$:

$$-(\mathscr{F}')_{\alpha=\alpha_{1,3}(c_2)} = \left\{\frac{1}{[\cos^3\alpha(\frac{7}{3}\sin^2\alpha - 1)]}\right\}_{\alpha=\alpha_{1,3}(c_2)}. \tag{A 5}$$

Appendix B

Introducing the function $f_p(\xi)$ in a parametric representation in terms of $\sin\alpha$ results in

$$f_{p\xi} = f_p'/\xi', \quad f_{p\xi\xi} = (f_p''\xi' - f_p'\xi'')/(\xi')^3 \tag{B 1}$$

where $(\,)' = \mathrm{d}(\,)/\mathrm{d}(\sin\alpha)$.

From (19), (21), (22) and (28):

$$f_\xi - \tfrac{36}{49}\xi^2 = -(\tfrac{3}{2})^{\frac{1}{3}} c_1^{\frac{2}{7}} \mathscr{F}^{\frac{2}{7}} \cos^{\frac{2}{3}}\alpha (1+S^2), \tag{B 2}$$

$$f_{\xi\xi} + \tfrac{6}{7}(2a-\tfrac{13}{7})\,\xi = -(\tfrac{3}{2})^{\frac{1}{3}} c_1^{\frac{1}{7}} \mathscr{F}^{\frac{1}{7}} \cos^{\frac{1}{3}}\alpha \frac{(2a-\frac{13}{7})S^2 + (2a-\frac{11}{7})S - \frac{2}{7}\tan\alpha}{1+S^2}, \tag{B 3}$$

where S is defined in (22b). Also, by a direct differentiation

$$\xi' = \tfrac{7}{3}(\tfrac{3}{2})^{\frac{1}{3}} c_1^{\frac{1}{7}} \mathscr{F}^{\frac{1}{7}} \cos^{-\frac{2}{3}}\alpha (1+S^2), \tag{B 4}$$

$$\xi'' = \tfrac{1}{2}(\tfrac{3}{2})^{\frac{1}{3}} c_1^{\frac{1}{7}} \mathscr{F}^{\frac{1}{7}} \cos^{-\frac{2}{3}}\alpha \left[\frac{14}{3}(1+S^2)\left(\frac{2}{3}\frac{\sin\alpha}{\cos^2\alpha} - \frac{13}{7}\frac{\mathscr{F}'}{\mathscr{F}}\right) + \frac{4}{3}\frac{\mathscr{F}'}{\mathscr{F}} + \frac{4}{7}\left(\frac{\mathscr{F}'}{\mathscr{F}}\right)^2 \sin\alpha\right], \tag{B 5}$$

where (15) for $\mathscr{F}$ is used to get simpler expressions. Equation (33) results from substituting (B 1)–(B 5) into (32a), rearranging the various terms and using (22).

Appendix C

The function $f_1(\xi)$ is introduced in a parametric representation in terms of $\sin\alpha$. Therefore, following the analysis in Appendix B, from (33) for $a = \frac{2}{7}$, the left-hand side in (50) becomes

$$\text{LHS} = \cos^2\alpha f_1'' - \tfrac{4}{3}\sin\alpha f_1' - \tfrac{10}{9} f_1 + \frac{4}{7}\frac{\mathscr{F}'\cos^2\alpha}{\mathscr{F}} f_1 - \frac{10}{49}\left(\frac{\mathscr{F}'\cos^2\alpha}{\mathscr{F}}\right)^2 f_1. \tag{C 1}$$

From (19), (21), (22) and (28):

$$(\tfrac{4}{7}f - \tfrac{6}{7}\xi f_\xi)^2 = c_1^{\frac{6}{7}} \mathscr{F}^{\frac{6}{7}} \sin^2\alpha \tag{C 2}$$

so the right-hand side of (50) becomes

$$\text{RHS} = 2(\tfrac{2}{3})^{\frac{1}{3}} c_1^{\frac{5}{7}} \mathscr{F}^{-\frac{2}{7}} \cos^{\frac{2}{3}}\alpha \{[1 + \tfrac{3}{4}(\gamma - \tfrac{1}{2})](\mathscr{F}'\sin^2\alpha + \tfrac{7}{3}\mathscr{F}\sin\alpha) - \tfrac{3}{4}(\gamma - \tfrac{1}{2})\mathscr{F}'\}, \tag{C 3}$$

where (B 4) for ξ' was also used. Now, following the assumption in (34) for $a = \frac{2}{7}$ results in (51a). The substitution of (C 1), (C 3) and (51a) in (50) results in (51b).

REFERENCES

Abbott, I. H. & Doenhoff, A. E. von 1959 *Theory of Wing Sections*. Dover.

Albone, C. M., Catherall, D., Hall, M. G. & Joyce, G. 1974 *RAE Tech. Rep.* 74056. An improved numerical method for solving the transonic small-disturbance equation for the flow past a lifting airfoil.

Bateman, H. 1953 *Higher Transcendental Functions*, vol. 1. McGraw-Hill.

Bauer, F., Garabedian, P., Korn, D. & Jameson, A. 1975 *Supercritical Wing Sections II*. Lecture Notes in Economics and Mathematical Systems, vol. 108. Springer.

Cole, J. D. 1991 Asymptotic theory in aerodynamics, *AIAA Paper* 91-0028.

Cole, J. D. & Cook, L. P. 1986 *Transonic Aerodynamics*. North-Holland.

Guderley, K. G. 1962 *The Theory of Transonic Flow*. Pergamon.

Hughes, T. J. R., Franca, L. P. & Hulbert, G. M. 1989 A new finite element formulation for computational fluid dynamics. VIII. The Galerkin least squares method for advective-diffusive equations. *Comput. Meth. Appl. Mech. Engng* **73**, 173–189.

Jameson, A. 1985 Transonic flow calculations. *Princeton University MAE Rep.* 1651.

Keyfitz, B. L., Melnik, R. E. & Grossman, B. 1978 An analysis of the leading-edge singularity in transonic small disturbance theory. *Q. J. Mech. Appl. Math.* **31**, 137–155.

KEYFITZ, B. L., MELNIK, R. E. & GROSSMAN, B. 1979 Leading-edge singularity in transonic small disturbance theory: numerical resolution. *AIAA J.* **17**, 296–298.

KUSUNOSE, K. 1979 Two-dimensional flow past convex and concave corners at transonic speed and two-dimensional flow around a parabolic nose at subsonic and transonic speeds. Ph.D thesis, University of California at Los Angeles, CA.

MÜLLER, E. A. & MATSCHAT, K. 1964 Ähnlichkeitslösungen der Transsonischen Gleichungen bei der Anström – Machzahl 1. In *Proc. 11th Intl Congr. Applied Mechanics, Munich, Germany* (ed. H. Görtler), pp. 1061–1068. Springer.

MURMAN, E. M. & COLE, J. D. 1971 Calculation of plane steady transonic flows. *AIAA J.* **9**, 114–121.

NONWEILER, T. R. F. 1958 The sonic flow about some symmetric half-bodies. *J. Fluid Mech.* **4**, 140–148.

RUSAK, Z. 1990 Subsonic flow around a thin airfoil with a parabolic nose. Dept. of Mathematics *Rep.* 186. Rensselaer Polytechnic Institute.

WEBSTER, B. E., SHEPHARD, M. S., RUSAK, Z. & FLAHERTY, J. E. 1992 An adaptive finite element method for rotorcraft aerodynamics. *7th IMACS Conf. on Computer Methods for Partial Differential Equations, Rutgers University* (ed. R. Vichnevetsky). Elsevier (in press).